Bootstrapping Quantum Gravitational Problems

Anish Suresh[1]
Advisor: Mukund Rangamani[2]

[1] *Department of Physics and Astronomy, Rutgers University, Piscataway, NJ, 08854*
[2] *QMAP & Department of Physics, University of California Davis, Davis, CA, 95616*

(Dated: January 13, 2025)

Abstract

The principle of holography, which states that a gravitational theory is closely related to a non-gravitational theory of lower dimension, has revolutionized the search for a theory of quantum gravity. One such example of this is the D0-Brane matrix model, which exhibits signatures of M-theory in specific conditions and is the holographic dual of a 10 dimensional black hole of type IIA string theory. Understanding the properties of this model is difficult to do analytically. In this report, we use the bootstrap method, a numerical technique that utilizes a positivity constraint to narrow down the range of allowed values. We consider many simple systems to provide a comprehensive review of the bootstrap method. We also bootstrap the D0-Brane matrix model and reproduce bounds on observables of that setting.

Keywords: Holography, D0-Brane Matrix Model, Bootstrap.

Contents

1. Introduction

Newton's formulation of physics reigned supreme for multiple centuries. When it seemed like our understanding of physics was complete, the works of Planck and Einstein turned this dusk into the dawn of a new era. The discovery of quantum mechanics and general relativity breathed new life into the field. These two subjects revolutionized our understanding of the world at minuscule and gargantuan scales, typically unreachable without technology. Quantum mechanics gave birth to the idea of discreteness of energy levels, which allowed for a much better understanding of particles. General relativity redefined gravity as the curvature of spacetime, which successfully accounted for existing problems like the precession of Mercury's perihelion, while predicting extreme objects such as black holes.

The beauty of both of these theories is their connection to the classical world. Simply taking the appropriate limits in both recovers Newton's formalism of classical mechanics. This makes sense, since each theory is a more general version of Newton's mechanics. It is then natural to try and combine all of these together into a unified theory. Quantum field theory weaves together special relativity and quantum mechanics, but the coalescence of general relativity with quantum mechanics poses a problem. One such example of their incompatibility can be seen in Hawking's paradox regarding black holes.

Quantum gravity is the field that aims to resolve this issue and combine both fields[1]. There has been considerable work done regarding this, giving birth to a myriad of theories that claim to do so. The most prevalent of these is string theory, in which the fundamental particles are vibrations on 1 dimensional objects known as strings [1].

In this ongoing search, Gerard 't Hooft and Leonard Susskind proposed an idea known as *holography*, which suggested that the degrees of freedom of our universe can be found on its boundary. In 1997, Juan Maldecena physically formulated this idea into the AdS/CFT correspondence, which related the gravitational Anti de Sitter (AdS) space with a lower dimensional non-gravitational conformal field theory (CFT) [2]. While we will not go into too much detail here (see [3, 4, 5] for comprehensive reviews), the important thing is that studying one of these theories provides insight on the other.

In this report, we discuss the D0-Brane matrix model (an alternate limit to the well-known BFSS model [6], relating it to M-theory), which is equivalent to a 10 dimensional charged black hole in type IIA string theory under the *'t Hooft limit*, by the gauge/gravity duality mentioned above. This model contains 9 bosons and 16 Majorana fermions, which are represented as $N \times N$ matrices with N being large. Our goal is to learn information about the quasinormal modes of the black hole through the matrix model theory. These modes have been found through the super-gravitational side already [7]. In addition, we would like to verify if this model has zero bound energy states, a conjecture that has been analytically proven for $N = 2$ but not for other Ns due to complexity. This is not surprising. When looking at the much simpler

[1]Technically, there are four forces that are involved, but three of these fall under the realm of quantum mechanics.

quantum mechanics, the evolution of every wave function ψ is dictated by the time-independent Schrödinger's equation:

$$H\psi = \left(\frac{p^2}{2m} + V(x)\right)\psi = \left(-\frac{1}{2m}\frac{\partial^2}{\partial x^2} + V(x)\right)\psi = E\psi, \tag{1}$$

where we assume natural units ($c = \hbar = 1$) for the rest of this report. The energy E, which are the eigenvalues of H, can only be found analytically for a handful of potentials [8]. Thus, numerical methods are virtually necessary to find the energy values of quantum mechanical systems - and hence the D0-Brane matrix model.

One such method is the *bootstrap method*. Most numerical methods, such as the Monte Carlo method, determine values by checking which values of sought-after parameters satisfy the given equations. On the other hand, the bootstrap method identifies regions of values that the parameters cannot take. These are done through derived relations and a positivity constraint; as the complexity/number[2] of constraints get larger, the 'incorrect' regions grow, leaving the allowed values. This technique, which was initially formulated to study the S-matrix [9, 10], has been found to be accurate in various settings, which we shall cover in this report. We specifically choose to work with this method because the Monte Carlo method has been shown to be quite complex in the D0-Brane matrix model. On the other hand, Henry Lin has found results similar to the Monte Carlo method using simple bootstrap constraints [11]. Thus, this technique may provide new insight on the model with more constraints.

In this report, we begin using the bootstrap method on single particle systems, such as the harmonic oscillator and the Pöschl-Teller potential. This also includes $\mathcal{PT}$-symmetric systems, which have non-Hermitian Hamiltonians. We work with Hamiltonians found in other articles, and are able to successfully reproduce their results. We then turn our attention towards quasinormal modes of black holes. We study three settings: the AdS_3 metric, Schwarzschild black hole, and the BTZ black hole. For the two 3 dimensional cases, we analytically find the quasinormal modes, while we apply a semi-analytical technique for the other. In addition, we attempt to apply the bootstrap method on the BTZ black hole, which fails due to the behavior of the 'potential' of its radial equation. We also discuss potential remedies for this issue. Next, we turn to bootstrapping matrix models. We start with the anharmonic oscillator, an example of one matrix quantum mechanics. We finally work with the D0-Brane matrix model and reproduce the results in Lin's paper.

This report is arranged as follows. Section 2 contains examples of single particle systems being bootstrapped. In Section 2.3, various $\mathcal{PT}$-symmetric systems are considered. The derivations for the quasinormal modes of black holes can be found in Section 3. Sections 3.4 and 3.5 deal with bootstrapping the BTZ black hole and discussing issues in our approach. We cover matrix models in Section 4, and an extensive look at the D0-Brane matrix model can be found in Section 4.2. We wrap up the report and conclude our thoughts in Section 5.

2. Single Particle Quantum Systems

Before we discuss large N matrix models, we turn to single particle quantum mechanics, where x and p are scalars. The constraints for this model can be found at the energy eigenstates $|E\rangle$. From basic quantum mechanics, we find that

$$\langle [H, \mathcal{O}] \rangle = 0, \tag{2a}$$
$$\langle H\mathcal{O} \rangle = E\langle \mathcal{O} \rangle, \tag{2b}$$

[2] The appropriate term depends on whether we are observing single particle systems or matrix models. This notion will become clear.

where H is the Hamiltonian of the system and $\mathcal{O}$ is any operator. Furthermore, the positivity of the norm gives us the positivity constraint:

$$\langle \mathcal{O}^\dagger \mathcal{O} \rangle \geq 0. \tag{3}$$

With the relations in eqns. (2a) and (2b), our goal is to derive a recursion relation for the expectation value of an operator. Such an expression will be able to generate a sequence of moments $\{\langle f(x)^n \rangle\}_{n=0}^K$ for some integer K, where $f(x)$ depends on the form of the potential $V(x)$. Using these, we can define the *Hankel* matrix as $\mathcal{M}_{ij} = \langle f(x)^{i+j} \rangle$. Then, we see that for $\mathcal{O} = \sum_{n=0}^K a_n f^n$, the positivity constraint states

$$0 \leq \langle \mathcal{O}^\dagger \mathcal{O} \rangle = \sum_{i,j=0}^K a_i^* \langle f(x)^{i+j} \rangle a_j = \sum_{i,j=0}^K a_i^* \mathcal{M}_{ij} a_j = \vec{a} \cdot M \vec{a}, \tag{4}$$

where $\vec{a} \in \mathbb{C}^n$. Thus, the positivity constraint states that this matrix must be positive semi-definite. This condition will determine the regions that E (among other parameters) cannot be in. As $K \to \infty$, this area will expand, and the remaining regions will correspond to the allowed energy eigenvalues.

To see this in motion, we bootstrap quantum systems with analytical solutions so that we can compare the analytical energy eigenvalues to ones found through the bootstrap method. Such a process will be informative in how to find the operator in the moments sequence and the dimension of the region to be bootstrapped.

2.1 Harmonic Oscillator

We begin with the harmonic oscillator potential due to its simplicity, and we were motivated to bootstrap this example to match the work in [12]. We independently rederived these results to test the Bootstrap method and compare our work with existing literature.

Here, the potential is $V(x) = \frac{1}{2}x^2$. Thus, it is reasonable to expect the moment sequence to be of the form $\{\langle x^n \rangle\}_{n=0}^\infty$. With this in mind, we can use $\mathcal{O} = x^n p$ with eqn. (2a) to find

$$n\langle x^{n-1}p^2 \rangle + \frac{1}{4}n(n-1)(n-2)\langle x^{n-3} \rangle - \langle x^{n+1} \rangle = 0. \tag{5}$$

To substitute out $\langle x^{n-1}p^2 \rangle$, we can use eqn. (2b) with $\mathcal{O} = x^{n-1}$ to get

$$\langle x^{n-1}p^2 \rangle = 2E\langle x^{n-1} \rangle - \langle x^{n+1} \rangle. \tag{6}$$

When combining these equations, we arrive at the recursion relation we are looking for:

$$\langle x^n \rangle = \frac{1}{n}\left(2E(n-1)\langle x^{n-2} \rangle + \frac{1}{4}(n-1)(n-2)(n-3)\langle x^{n-4} \rangle\right), \tag{7}$$

where we rescaled n by $n \to n-1$.

To initialize this relation, we set $\langle x^0 \rangle = 1$. In addition, we know that the expectation values of odd powers of x are 0, since the potential is even[3]. Nothing else can be said about the other moments. Thus, we plug in increasing values of n to determine if there are any moments that cannot be written as a function of other moments and E. We see that when $n = 2$, $\langle x^2 \rangle$ is purely a function of E. Thus, our *search space* S, the set of initial conditions, is just $\{E\}$.

[3]This fact is also discernible from the recursion relation. When $n = 1$, eqn. 7 reads $\langle x \rangle = 0$. For all odd natural numbers beyond $n = 1$, the equation similarly reads 0, since $\langle x^n \rangle$ depends on $\langle x \rangle, \langle 3 \rangle, \cdots, \langle x^{n-2} \rangle$.

We can now construct our Hankel matrix. We automated this process on *Mathematica*. Such a matrix for $K = 5$ is the following:

$$\mathcal{M} = \begin{pmatrix} 1 & 0 & E & 0 & \frac{3E^2}{2} + \frac{3}{8} \\ 0 & E & 0 & \frac{3E^2}{2} + \frac{3}{8} & 0 \\ E & 0 & \frac{3E^2}{2} + \frac{3}{8} & 0 & \frac{5E^3}{2} + \frac{25E}{8} \\ 0 & \frac{3E^2}{2} + \frac{3}{8} & 0 & \frac{5E^3}{2} + \frac{25E}{8} & 0 \\ \frac{3E^2}{2} + \frac{3}{8} & 0 & \frac{5E^3}{2} + \frac{25E}{8} & 0 & \frac{35E^4}{8} + \frac{245E^2}{16} + \frac{315}{128} \end{pmatrix}. \tag{8}$$

Since our search space is one-dimensional, we can easily work with higher values of K. Thus, we consider $K = 11, 21$ for this example. With their Hankel matrices constructed, we can simply find values of E for which all the eigenvalues are non-negative. The plots of E depicting the 'allowed' energy eigenvalues can be found in Figure 1. It is easy to see that $K = 21$ does a better job at finding these values, which we know analytically are $E_n = \frac{n}{2}$ for odd, natural numbers n. As higher values of K are used, the bootstrap method will yield better results.

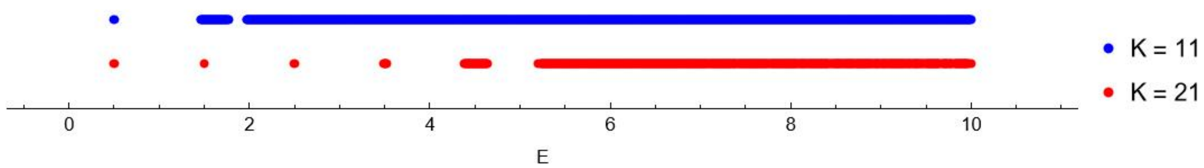

Figure 1: A plot of the allowed energy eigenvalues of the harmonic oscillator for $K = 11$ (orange, upper) and $K = 21$ (purple, lower). Note that $K = 11$ only produces the $E = 1/2$ value, with the rest being hazy. $K = 21$ also has this haze for $E > 5$, but it successfully finds $E = 1/2, 3/2, 5/2$, and $7/2$.

We can now turn to a more complicated example.

2.2 Pöschl-Teller Potential

The Pöschl-Teller potential is $V(x) = \frac{-\lambda(\lambda+1)}{2}\text{sech}^2(x)$, where $\lambda \in \mathbb{Z}^+$. This potential is a great example, since it serves as a complex example to bootstrap. Furthermore, experience with this system will prove useful in studying gravity, as we shall see in Section 3.4.

Here, it is natural to derive a recursion relation for the sequence $\{\langle \text{sech}^n(x)\rangle\}_{n=0}^{\infty}$. We can begin with $\mathcal{O} = \text{sech}^n(x)\tanh(x)p$ in eqn. (2a), which yields

$$\begin{aligned} &-\frac{1}{2}\Big[n^2\langle \text{sech}^n(x)\tanh(x)p\rangle - (n+1)(n+2)\langle \text{sech}^{n+2}(x)\tanh(x)p\rangle\Big] \\ &-i\Big[(n+1)\langle \text{sech}^{n+2}(x)p^2\rangle - n\langle \text{sech}^n(x)p^2\rangle\Big] + 2iV_0(\langle \text{sech}^{n+4}(x)\rangle - \langle \text{sech}^{n+2}(x)\rangle) = 0. \end{aligned} \tag{9}$$

Note the $\langle \cdots p\rangle$ term that appears here, but not in the harmonic oscillator case. To get rid of this term, along with the $\langle \cdots p^2\rangle$ term, we can use $\mathcal{O} = \text{sech}^n(x)$ in both eqns. (2a and (2b)) to find

$$\begin{aligned} \langle \text{sech}^n(x)\tanh(x)p\rangle &= \frac{i}{2}\Big[(n+1)\langle \text{sech}^{n+2}(x)\rangle - n\langle \text{sech}^n(x)\rangle\Big], \\ \langle \text{sech}^n(x)p^2\rangle &= 2E\langle \text{sech}^n(x)\rangle - 2V_0\langle \text{sech}^{n+2}(x)\rangle. \end{aligned} \tag{10}$$

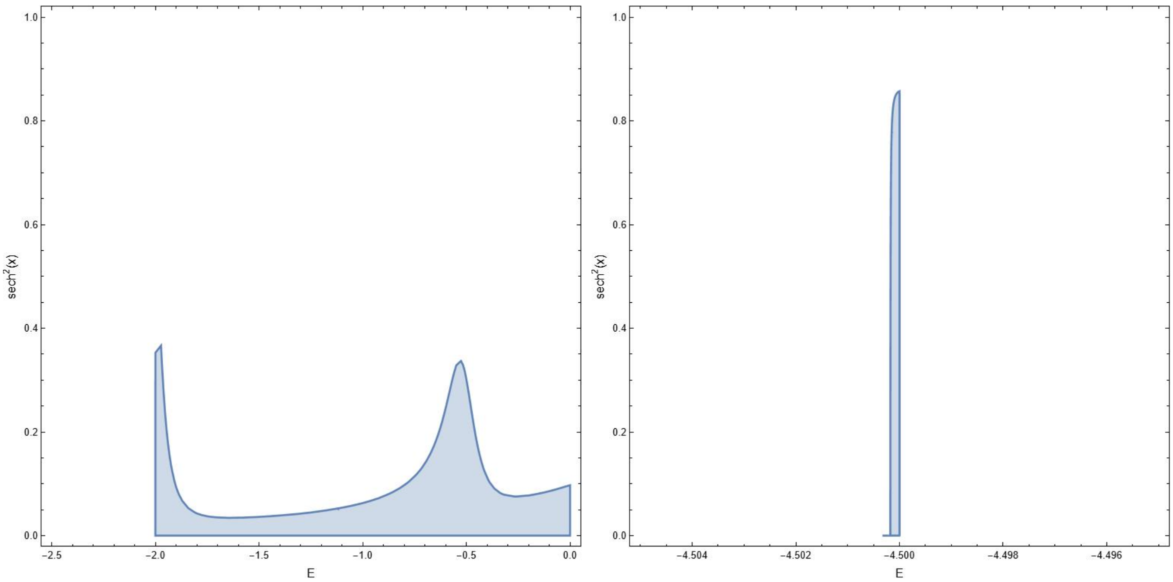

Figure 2: Plots of the bootstrapped regions of the Pöschl-Teller potential with $K = 7$ and $\lambda = 3$. Here, we can observe peaks at $E = -1/2, -2$, and $-9/2$, which match the analytical energy values. Note that a zoom-in to find the $-9/2$ energy state was needed.

Combining both of these relations gives us the recursion relation:

$$\begin{aligned} &-\frac{1}{4}(n+2)(-2\lambda+n+1)(2\lambda+n+3)\langle \operatorname{sech}^{n+4}(x)\rangle = \\ &\left(2En+\frac{n^3}{4}\right)\langle \operatorname{sech}^{n}(x)\rangle - \frac{1}{2}(n+1)\left(-2\lambda^2-2\lambda+n^2+2n+4e+2\right)\langle \operatorname{sech}^{n+2}(x)\rangle. \end{aligned} \tag{11}$$

Like the previous example, the potential is even, so all odd powered moments must be 0. The search space is thus $\{E, \langle \operatorname{sech}^2(x)\rangle\}$, since we do not want $\langle \operatorname{sech}^{-2}(x)\rangle$ in our recursion relation. Thus, our search space is two-dimensional, making this problem more computationally complex.

We can counter this issue with a simple trick: since $\langle \operatorname{sech}^{2n+1}(x)\rangle = 0$ for $n \in \mathbb{N}$, we can make our sequence $\langle (\operatorname{sech}^2(x))^n\rangle_{n=0}^{\infty}$. That is, we can set $n = 2s-4$ such that eqn. (11) becomes

$$r_s = -\frac{(4Es - 8e + 2s^3 - 12s^2 + 24s - 16)\, r_{s-2} + (-4Es + 6E - 4s^3 + 18s^2 - 4s - 21)\, r_{s-1}}{2s^3 - 6s^2 - \frac{37s}{2} + \frac{45}{2}}, \tag{12}$$

where $r_s = \langle (\operatorname{sech}^2(x))^s\rangle$. Making this substitution reduces the size of the Hankel matrix in this situation, hence reducing the complexity. The result of using bootstrap on this recursion relation for $\lambda = 3$ and $K = 7$ can be found in Figure 2. In general, the eigenvalues of this system are $\{-\frac{n^2}{2}\}_{n=1}^{\lambda}$. It can be seen in Figure 2 that the bootstrap method is successful in retrieving the energy values $-1/2, -2$, and $-9/2$. It is worth noting that the $E = -9/2$ value had to be found through zooming in quite closely and adding `PlotPoints` $\to$ 100 when plotting. This extra effort needed can possibly be attributed to bootstrap converging to this energy eigenvalue too fast. Such energy levels may prove difficult to find for models that have an unknown eigenvalues.

After observing the success of the bootstrap method for these examples, we can test this method on the more non-traditional theory of $\mathcal{PT}$ symmetric systems.

2.3 $\mathcal{PT}$ Symmetric Systems

Before we understand the bootstrap constraints of $\mathcal{PT}$ symmetric Hamiltonians, let us provide a brief introduction to the topic. It is well known that the Hamiltonian H of quantum mechanics dictates the energy states and the time evolution of states. Mathematically, these conditions state that the eigenvalues of H are real and e^{-iHt} is unitary, which are necessary conditions to ensure the theory is physical. If H is Hermitian, then it is easy to see that these requirements are satisfied. However, Hermiticity is not the only property of the Hamiltonian that satisfies these requirements.

One of the causes of such an idea was a conjecture made by D. Bessis [13], which stated that the eigenvalues of $H = p^2 + x^2 + ix^3$, which is not Hermitian, were real and positive. This claim, which was formed on the basis off of numerical means, could be attributed to the $\mathcal{PT}$ symmetry, or both parity (spatial reflections) and time reversal, of the Hamiltonian. More specifically, when making the transformations (i) $i \to -i$ and (ii) $x \to -x$, this Hamiltonian remains invariant[4]. Such Hamiltonians have been shown to produce real eigenvalues and unitary time operators [13, 14]. There is still work being done on extracting observables of $\mathcal{PT}$-symmetric Hamiltonians, but they have been found to describe interacting systems [15, 16].

Our motivation to study the effect of the bootstrap method on $\mathcal{PT}$-symmetric systems is to simply illustrate the range of the technique. The general process remains the same. However, a slight modification of constraints in eqns. (2a), (2b), and (3) is required to execute this method in this setting. We will illustrate the changes needed for the constraints, but not explicitly derive the recursion relations like before, since that process is identical to the Hermitian case.

Like before, we have that $H|E_n\rangle = E_n|E_n\rangle$. However, we now see that $\langle E_n|H^\dagger = \langle E_n|E_n^* \neq \langle E_n|E_n$. Such a property becomes problematic when deriving the aforementioned constraints. Thus, we introduce a new operator $\mathcal{V} = e^{\mathcal{Q}}$ [17] that is Hermitian, positive, $\langle \mathcal{V} \rangle = 1$, and satisfies[5] $H^\dagger = \mathcal{V} H \mathcal{V}^{-1}$. Thus, it is easy to see that we have the following constraints:

$$\langle [H, \mathcal{O}] \rangle_{\mathcal{V}} = \langle \mathcal{V}[H, \mathcal{O}] \rangle = 0, \tag{13a}$$
$$\langle H\mathcal{O} \rangle_{\mathcal{V}} = \langle \mathcal{V} H \mathcal{O} \rangle = E \langle \mathcal{O} \rangle_{\mathcal{V}}, \tag{13b}$$
$$\langle \mathcal{V}^{-1} \mathcal{O}^\dagger \mathcal{V} \mathcal{O} \rangle_{\mathcal{V}} = \langle \mathcal{O}^\dagger \mathcal{V} \mathcal{O} \rangle \geq 0, \tag{13c}$$

where $\langle X \rangle_{\mathcal{V}} = \langle \mathcal{V} X \rangle$. Note that if $\mathcal{V}^{-1}\mathcal{O}^\dagger\mathcal{V} \sim \mathcal{O}^\dagger$, then all of the constraints are identical to ones from Hermitian quantum mechanics. Such an equivalence can be found given the nature of x and p, as we shall see for a couple of examples.

2.3.1 Shifted Harmonic Oscillator

The Hamiltonian here is

$$H = p^2 + x^2 + 2i\epsilon x. \tag{14}$$

It is easy to see that the last term is what makes the Hamiltonian $\mathcal{PT}$-symmetric and not Hermitian. Thus, to determine $\mathcal{Q}$ - and hence $\mathcal{V}$ - such that $H^\dagger = \mathcal{V} H \mathcal{V}^{-1}$, we need $\mathcal{Q}$ to be a function of momentum along; otherwise, the position operators would commute, indicating a false Hermiticity of the Hamiltonian. Since the term of concern is linear in position, it is worth considering $\mathcal{Q} = \alpha p$.

Applying the commutation relation $[p^n, x] = -inp^{n-1}$, we find the following constraint on α:

$$-2ix\alpha - \alpha^2 + x^2 + 2ix + 2\epsilon\alpha = x^2 - 2i\epsilon x. \tag{15}$$

[4] Note that this Hamiltonian is not $\mathcal{P}$ and $\mathcal{T}$ symmetric individually. That is, parity $\mathcal{P}$ has the effect of (i) $x \to -x$ and (ii) $p \to -p$, while time reversal $\mathcal{T}$ makes (i) $p \to -p$ and (ii) $i \to -i$.

[5] This property allows one to tie a $\mathcal{PT}$-symmetric Hamiltonian to a Hermitian Hamiltonian, since $\mathcal{H} = e^{-\mathcal{Q}/2} H e^{\mathcal{Q}/2}$ is Hermitian (however, this changes the boundary conditions, meaning the solutions may be affected). Thus, the $\mathcal{V}$ operator is important in understanding the role of observables in $\mathcal{PT}$-symmetric models [14].

Grouping the terms with and without x and solving for α yields $\alpha = 2i\epsilon$[6], meaning $\mathcal{Q} = 2i\epsilon p$ and $\mathcal{V} = e^{2i\epsilon p}$. Note that setting $\epsilon = 0$ makes $\mathcal{V} = \mathbb{1}$, which makes sense as Hermiticity is restored. Moreover, it is easy to check that $\mathcal{V}$ in general satisfies all of its above properties.

This means that $\mathcal{V}^{-1}p\mathcal{V} = p$, which cannot be said about x. Thus, the positivity constraint here, given $\mathcal{O} = \sum_{n=0}^{K} a_n p^n$, reads

$$0 \leq \langle \mathcal{V}^{-1}\mathcal{O}\mathcal{V}\mathcal{O}\rangle_{\mathcal{V}} = \sum_{i,j=0}^{K} a_i^* \langle p^{i+j}\rangle_{\mathcal{V}} a_j. \tag{16}$$

Like before, we can define $\mathcal{M}_{ij} = \langle p^{i+j}\rangle_{\mathcal{V}}$ and carry on the bootstrap method. It is important to note that $\langle\cdots\rangle_{\mathcal{V}}$ is the analog of $\langle\cdots\rangle$ in the $\mathcal{PT}$-symmetric setting. The derivation of the recursion relation is identical to the Hermitian setting because all of the constraints use this specific type of expectation value. However, there may be a change in the domains of search space parameters; that is, $\langle x\rangle$ and $\langle \mathcal{V}x\rangle$ may make the Hankel matrix positive semi-definite at different values. No such difference was found for the $\mathcal{PT}$-symmetric Pöschl-Teller potential, which had an identical recursion relation to the one derived in Section 2.2 [19].

When using the bootstrap method with the recursion relation found in [19], we produce plots that match the results of that paper. These can be found in Figure 3.

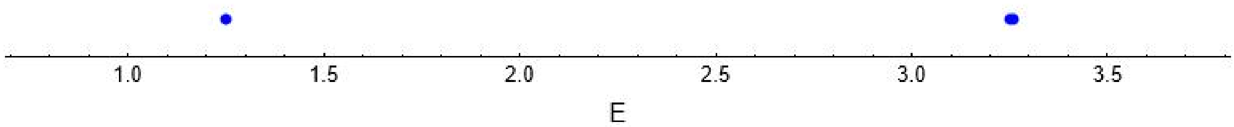

(a) Plot of the allowed energy eigenvalues found through bootstrap for $\epsilon = 0.5$ and $K = 15$. The expected values are 1.12 and 3.25, which matches the values found.

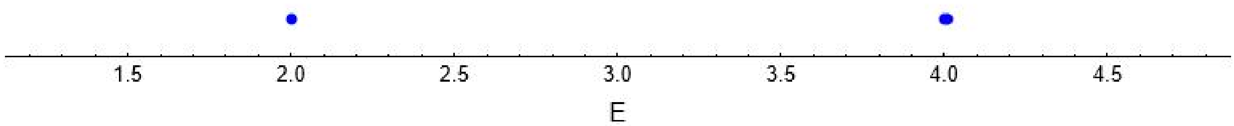

(b) Plot of the allowed energy eigenvalues found through bootstrap for $\epsilon = 1$ and $K = 15$. The expected values are 2 and 4, which matches the values found.

Figure 3

2.3.2 Swanson Hamiltonian

Here, the Hamiltonian is $H = p^2 + x^2 + ic\{x, p\}$, where $\{\cdot\}$ are the anticommutator brackets. Since the $\mathcal{PT}$-symmetric term is $\sim xp$, it is a good guess to assume $\mathcal{Q} = \alpha x^2$. Using the same process as before, it is easy to find that $\alpha = -c$. Since $\mathcal{V}$ is purely a function of x, meaning $\mathcal{V}^{-1}x\mathcal{V}$, so it is best to choose $\langle x^n\rangle_{\mathcal{V}}$ as our moment sequence. This is straightforward to find [18]. Figure 4 contains the energy levels found through bootstrap for this setting. It is worth noting that a deeper search was needed to accurately find intervals for each of the energy eigenvalues; that is, a step size of 10^{-2} proved insufficient, so we resorted to 10^{-3}.

For both the shifted harmonic oscillator and Swanson Hamiltonians, it is easy to see that the Hamiltonians become the harmonic oscillator when ϵ or c are set to 0. This can also be seen in the recursion relations in [19], as taking these limits produces the recursion relation in eqn. (7). This point illustrates that the derivation of the recursion relation is robust to additional terms.

[6]The equations with and without x produce the same value of α, which is a quirk that is interesting. This also happens for more complex systems, as commented in [18].

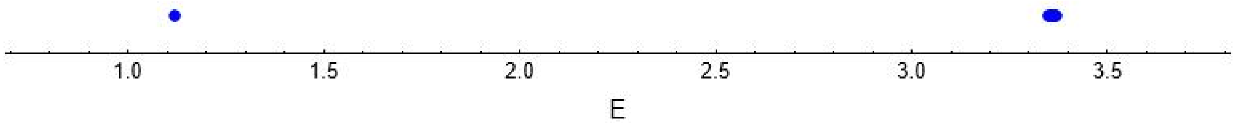

(a) Plot of the allowed energy eigenvalues of the Swanson Hamiltonian found through bootstrap for $c = 0.5$ and $K = 15$. The expected values are 1.12 and 3.35, which matches the values found.

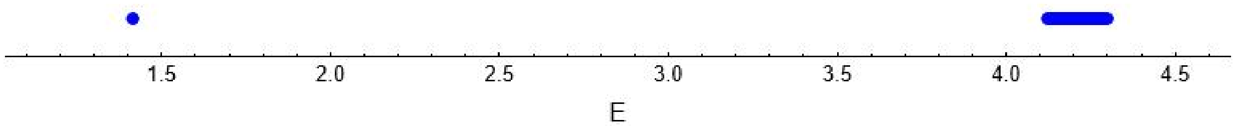

(b) Plot of the allowed energy eigenvalues found through bootstrap for $c = 1$ and $K = 12$. The expected values are 1.41 and 4.24, which matches the values found.

Figure 4

2.3.3 $V(x) = -x^4$

A more complex example is the Hamiltonian $H = p^2 - x^4$. The potential is clearly unbounded below. However, this Hamiltonian can be transformed into a solvable, $\mathcal{PT}$-symmetric Hamiltonian if x is on a contour in the complex world [13, 20, 19]:

$$H = \frac{1}{2}\{(1 + ix, p^2)\} - \frac{1}{2}p - 16(1 + ix)^2, \tag{17}$$

where $\{\cdot, \cdot\}$ are the anti-commutator brackets. Finding $\mathcal{Q}$ here is trickier, but since most of the $\mathcal{PT}$-symmetric terms are of x, it is wise to assume $\mathcal{Q}$ is a function of p. Namely, this operator is $p^3/48 - 2p$ [20]. Like the shifted harmonic oscillator example, the sequence of moments is $\langle p^n \rangle_{\mathcal{V}}$. Bootstrapping the recursion relation, which produces a three-dimensional search space, produces the plots in Figure 5, which showcase the ground and first excited energy levels. These roughly match the plots in [19], the difference in which could be attributed to different programming languages used to bootstrap.

As mentioned earlier, this example contains a three-dimensional search space, making it the most computationally intensive example provided thus far. Not only does this make a simple search take longer, but for recursion relations with unbounded moments, determining the area where the positivity constraint is satisfied becomes much more difficult. That is, there is no information on $\langle p^2 \rangle_{\mathcal{V}}$ and $\langle p \rangle_{\mathcal{V}}$, two elements of the search space. However, if the moment is bounded, like certain trigonometric or hyperbolic functions, then the region to search for those is bounded. For example, in Section 2.2, $\langle \operatorname{sech}^2(x) \rangle$ is bounded in the interval $[0, 1]$, so the area searched during bootstrap was designated to that region.

With the success of the bootstrap method in Hermitian and $\mathcal{PT}$-symmetric quantum mechanics, we can turn our attention to gravity. After all, holography suggests there is a connection between gravity and quantum mechanics.

3. Quasinormal Modes of Various Metrics

Let us briefly introduce quasinormal modes before deriving them for gravitational settings. Quasinormal modes are oscillations of a system that are dampened. These can be thought of as normal modes, along with an exponential term that dampens them based on some initial condition. That is, if a normal mode is given as $\mathrm{Re}(e^{i\omega_n t})$, where ω_n is the normal mode frequency, then the quasinormal mode is given by:

$$\varphi(t) = e^{\omega_d t}\mathrm{Re}(e^{i\omega_n t}). \tag{18}$$

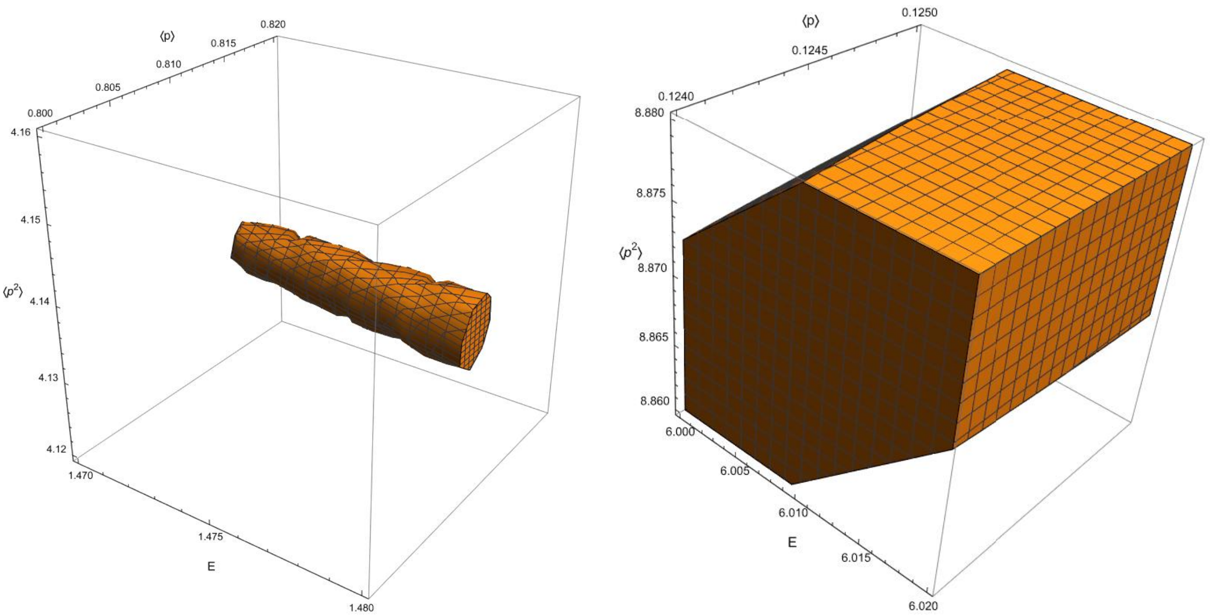

Figure 5: Plots of the ground state (left) and first excited (right) energy values of eqn. (17), as functions of E, $\langle p \rangle_{\mathcal{V}}$, and $\langle p^2 \rangle_{\mathcal{V}}$. Here, $K = 10$ to reduce complexity, and the intervals chosen for the search space parameters were based on the choices in [19]. This was done for the purpose of comparison.

.

It is clear that ω_d is a negative term that dictates the rate of decay of the normal mode that comes after it. We can rearrange the above equation into a form that is analogous to the normal mode wavefunction:

$$\varphi(t) = e^{\omega_d t}\mathrm{Re}(e^{i\omega_n t}) = \mathrm{Re}(e^{i(\omega_n - i\omega_d)t}) = \mathrm{Re}(e^{i\omega t}). \tag{19}$$

Thus, the quasinormal mode frequency ω is a parameter that incorporates both the normal mode frequency and the time decay parameter. Whether a system has normal or quasinormal modes is based on the boundary conditions at play. However, these conditions do not have to be based on time in general; a system's normal modes do not decay with respect to time unless some external force or object influences it. In fact, the one non-black hole example that we consider has normal modes, while the black hole metrics produce quasinormal modes. As we shall see below, the radial boundary conditions are what allows us to solve for the (quasi)normal mode frequencies.

When applied to black holes and gravitational metrics, (quasi)normal modes refer to how perturbations of the field in those metrics behave. We determine the (quasi)normal modes of three well-known metrics with a massless scalar field[7]. We do this analytically, but if such a process is not possible, then we will resort to semi-analytical means. This process can roughly be summed up as solving for the wave equation of GR from the Klein-Gordon operator:

$$\frac{1}{\sqrt{|\det g_{\mu\nu}|}}\partial_\mu(\sqrt{|\det g_{\mu\nu}|}g^{\mu\nu}\partial_\nu\phi) = 0. \tag{20}$$

We then use boundary conditions to determine how the time parameter behaves, which yield the modes. Thus, determining (quasi)normal mode frequencies of gravitational settings is simply a spectral/eigenvalue problem with initial values. As stated prior, the D0-Brane Matrix Model describes a black hole in the 't Hooft limit. Studying the certain correlation functions of the

[7] Using different fields, such as a massive scalar field or a electromagnetic field, yield different modes. However, the flavor of the problem is the same regardless, so we stick to working with the simplest case.

this model provides insight on quasinormal modes frequencies of this black hole. As such, a thorough review of quasinormal modes in simpler settings is key.

3.1 AdS$_3$ Metric

We begin with the AdS$_3$ spacetime. This is an example of a simple, gravitational spacetime that will produce normal and not quasinormal modes because there is no black hole present. Its metric is given by:

$$\mathrm{d}s^2 = -\left(\frac{r^2+l^2}{l^2}\right)\mathrm{d}t^2 + \left(\frac{l^2}{r^2+l^2}\right)\mathrm{d}r^2 + \left(r^2\right)\mathrm{d}\phi^2, \tag{21}$$

where l is the radius of AdS$_3$. This metric is diagonal in the $\{t, r, \phi\}$ coordinates, so our wave equation simplifies to

$$\frac{1}{r}\partial_\mu\left(r g^{\mu\mu}\partial_\mu\varphi\right) = 0. \tag{22}$$

Making the summation explicit, we arrive at at the partial differential equation we must solve:

$$-\left(\frac{l^2}{r^2+l^2}\right)\partial_t^2\varphi + \frac{1}{rl^2}\partial_r\left((r^3+l^2r)\partial_r\varphi\right) + \left(\frac{1}{r^2}\right)\partial_\phi^2\varphi = 0. \tag{23}$$

We can proceed to solve this partial differential equation through separation of variables. Through this, we find that $T(t) = e^{-i\omega t}$, since the perturbation vanishes as $t \to \infty$, and $\Phi(\phi) = e^{im\phi}$. It is important to note that ω are the mode frequencies that we are attempting to find. These should be real because they are normal mode frequencies. The radial equation turns out to be:

$$\frac{(r^2+l^2)^2}{l^4}R'' + \frac{(3r^2+l^2)(r^2+l^2)}{rl^4}R' + \left(-\frac{m(r^2+l^2)}{r^2l^2} + \omega^2\right)R = 0. \tag{24}$$

This equation can be solved explicitly. Before we do so, we rewrite our radial equation in terms of a new variable $z = \frac{r^2}{r^2+l^2}$. The motivation for this, originally inspired by the work in [21], will become apparent soon. The differential equation now reads:

$$z(1-z)R''(z) + (1-z)R'(z) + \left(-\frac{m^2}{4z} + \frac{l^2\omega^2}{4}\right)R(z) = 0. \tag{25}$$

Using `DSolve` in Mathematica, we can analytically solve this equation:

$$\begin{aligned} R(z) =& c_1 z^{-m/2}\,{}_2F_1\left(-\frac{m}{2} - \frac{l\omega}{2}, \frac{l\omega}{2} - \frac{m}{2}; 1-m; z\right) \\ &+ c_2 z^{m/2}\,{}_2F_1\left(\frac{m}{2} - \frac{l\omega}{2}, \frac{m}{2} + \frac{l\omega}{2}; m+1; z\right), \end{aligned} \tag{26}$$

where ${}_2F_1(a,b;c;x) = \sum_{n=0}^{\infty}\frac{(a)_n(b)_n}{(c)_n}\frac{x^n}{n!}$ is the hypergeometric function. Here, $(a)_n = \frac{\Gamma(a+n)}{\Gamma(n)}$ is the Pochhammer symbol. Since no horizon exists here, as $r = 0$ is the only singularity in the metric, we can use the fact that the wave must be smooth at $r = 0 \leftrightarrow z \to 0$. Each of the hypergeometric functions reduce to constants, so c_1 has to be 0 for smoothness. Thus, the radial solution is

$$R(z) = c_1 z^{m/2}\,{}_2F_1\left(\frac{m}{2} - \frac{l\omega}{2}, \frac{m}{2} + \frac{l\omega}{2}; m+1; z\right). \tag{27}$$

To retrieve the normal mode frequencies, we can use the other boundary condition: the wave must disappear as $r \to \infty \leftrightarrow z \to 1$. We can use a relation of hypergeometric functions, which we originally found in [21], that reads:

$$\begin{aligned} F(a,b;c;z) =& \frac{\Gamma(c)\Gamma(c-a-b)}{\Gamma(c-a)\Gamma(c-b)} F(a,b;a+b-c+1;1-z) \\ &+ (1-z)^{c-a-b} \frac{\Gamma(c)\Gamma(a+b-c)}{\Gamma(a)\Gamma(b)} F(c-a,c-b;c-a-b+1;1-z), \end{aligned} \tag{28}$$

where $a = \frac{m}{2} - \frac{l\omega}{2}, b = \frac{m}{2} + \frac{l\omega}{2}$, and $c = m + 1$. This is why we switched to the z coordinate; in this limit, $1 - z \to 0$, the hypergeometric functions are constants yet again. The second term vanishes in this limit. Thus, the only way for our radial solution to vanish in the far-field limit is if $\frac{\Gamma(c)\Gamma(c-a-b)}{\Gamma(c-a)\Gamma(c-b)} = 0$. This is only possible when $c - a = -n$ or $c - b = -n$ for $n \in \mathbb{N}_0$, meaning our normal mode frequencies are

$$\omega_n = \left| \pm \left(\frac{m + 2(n+1)}{l} \right) \right| = \frac{m + 2(n+1)}{l}. \tag{29}$$

Figure 6 shows $R(r)$ for select values of m and n. The normal modes of perturbations in AdS_3 spacetime are the total wavefunction, which are the product of time, angular, and radial functions:

$$\varphi(t,r,\phi) = \mathrm{Re}(e^{-i\omega_n t} e^{im\phi}) \left(\frac{r^2}{r^2 + l^2} \right)^{m/2} {}_2F_1 \left(\frac{m}{2} - \frac{l\omega_n}{2}, \frac{m}{2} + \frac{l\omega_n}{2}; m+1; \frac{r^2}{r^2 + l^2} \right) \tag{30}$$

up to some arbitrary constant in front. The mode frequencies are real, confirming these modes as normal. In fact, the frequencies above can be mapped to the energy levels of the quantum harmonic oscillator, since they are both evenly spaced.

Now, let us turn towards the BTZ black hole, which is a black hole in the AdS_3 spacetime.

3.2 BTZ Black Hole

The metric of the BTZ black hole spacetime is:

$$\mathrm{d}s^2 = -\left(\frac{r^2 - r_+^2}{l^2} \right) \mathrm{d}t^2 + \left(\frac{l^2}{r^2 - r_+^2} \right) \mathrm{d}r^2 + \left(r^2\right) \mathrm{d}\phi^2, \tag{31}$$

with $r_+ > 0$. The metric considered in the above section is identical to this one, given $r_+ = il$. Given the physical significance of this metric, we expect to find quasinormal modes here. Like before, we need to solve eqn. (20), which is identical to eqn. (22) from the previous section. Expanding this out leads to the following partial differential equation:

$$-\left(\frac{l^2}{r^2 - r_+^2} \right) \partial_t^2 \varphi + \frac{1}{rl^2} \partial_r \left((r^3 - r_+^2 r) \partial_r \varphi \right) + \left(\frac{1}{r^2} \right) \partial_\phi^2 \varphi = 0. \tag{32}$$

Using separation of variables, which yields the same solutions for t and ϕ as the AdS_3 spacetime, we find the radial equation:

$$\frac{(r^2 - r_+^2)^2}{l^4} R'' + \frac{\left(3r^2 - r_+^2\right)\left(r^2 - r_+^2\right)}{rl^4} R' + \left(-\frac{m(r^2 - r_+^2)}{r^2 l^2} + \omega^2 \right) R = 0. \tag{33}$$

In the AdS_3 setting, we then rewrote the radial equation in terms of a new variable z. We do this again with $z = 1 - \frac{r_+^2}{r^2}$ such that z is bounded between 0 and 1 [21]. The radial equation is now succinctly expressed as:

$$(1-z)zR''(z) + (1-z)R'(z) + \frac{R(z)\left(l^4\omega^2 - l^2 m^2 z\right)}{4r_+^2 z} = 0. \tag{34}$$

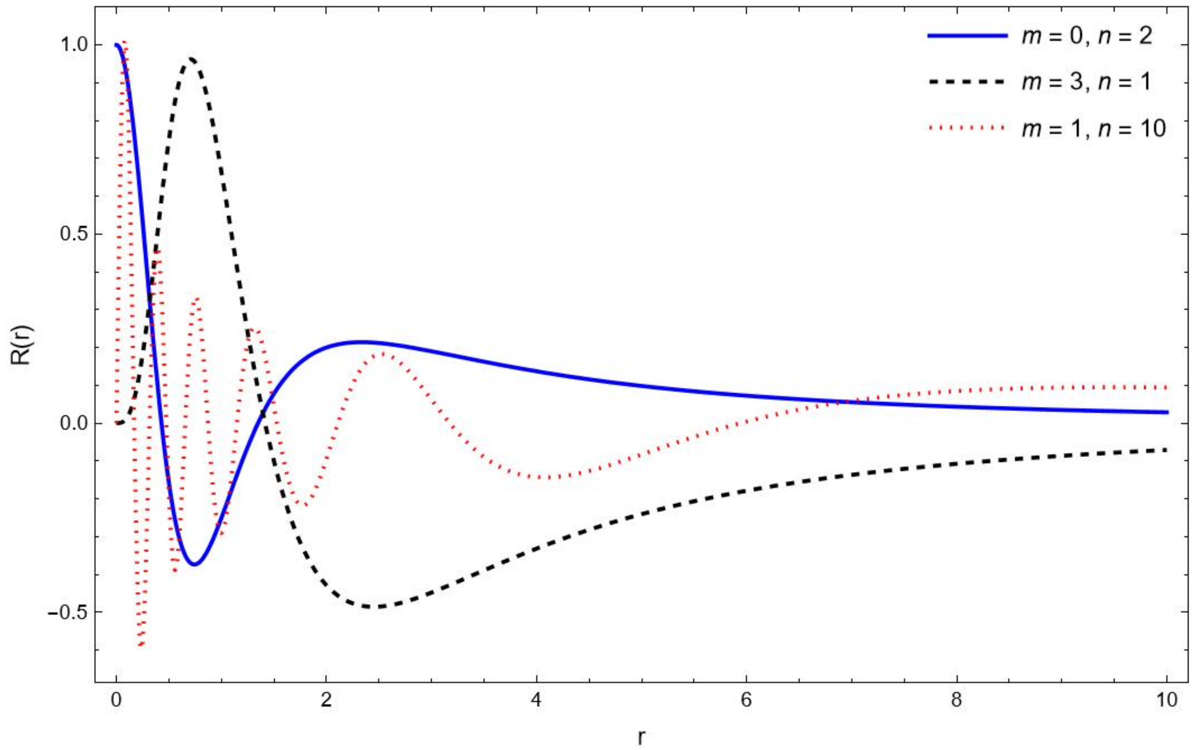

Figure 6: Plot of $R(r)$ from eqn. (27) for $(m, n) = (0, 2), (3, 1)$, and $(1, 10)$. A factor of $c_1 = 1, 15$, and 20 were respectively chosen for visibility.

This equation is exactly solvable, giving the solutions:

$$\begin{aligned} R(z) =& c_1 z^{-\frac{il^2\omega}{2r_+}} {}_2F_1\left(-\frac{i\omega l^2}{2r_+} - \frac{iml}{2r_+}, \frac{ilm}{2r_+} - \frac{i\omega l^2}{2r_+}; 1 - \frac{i\omega l^2}{r_+}; z\right) \\ &+ c_2 z^{\frac{il^2\omega}{2r_+}} {}_2F_1\left(\frac{il^2\omega}{2r_+} - \frac{ilm}{2r_+}, \frac{i\omega l^2}{2r_+} + \frac{iml}{2r_+}; \frac{i\omega l^2}{r_+} + 1; z\right). \end{aligned} \tag{35}$$

We must invoke boundary conditions once again to determine which of these two linearly independent solutions is correct. Since the horizon exists in this scenario, the wave at the horizon must be in-going. That is, when written in the tortoise coordinate[8] x, the wave must be of the form $\varphi(t, x, \phi) = e^{-i\omega(t+x)}e^{m\phi}$. Note that $r \to r_+$ means $z \to 0$. Furthermore, $dx/dr = l^2/(r^2 - r_+^2)$, so $x = \frac{l^2}{2r_+}\log\left(\frac{r-r_+}{r+r_+}\right)$. Then, we see that

$$e^{-i\omega x} \propto (r - r_+)^{-il^2\omega/2r_+}, \tag{36}$$

so the correct solution is the first one in eqn. (35).

The process for deriving the quasinormal modes is identical to the AdS_3 setting. Using the same far-field boundary condition, which states that the perturbation must vanish when $r \to \infty \leftrightarrow z \to 1$, and the hypergeometric function relation from eqn. (28), the radial solution becomes:

$$R(z) \to c_1 \frac{\Gamma(c)\Gamma(c-a-b)}{\Gamma(c-a)\Gamma(c-b)} F(a, b; a+b-c+1; 1-z), \tag{37}$$

where $a = -\frac{i\omega l^2}{2r_+} - \frac{iml}{2r_+}, b = \frac{ilm}{2r_+} - \frac{i\omega l^2}{2r_+}$, and $c = 1 - \frac{i\omega l^2}{r_+}$. Like before, this forces $c - a$ or $c - b$ to

[8]Such a set of coordinates, named after the well-known Zeno's paradox of Achilles and a tortoise, is commonplace when studying black hole spacetimes. In tortoise coordinates, radial null geodesics are surfaces in which time is considered constant.

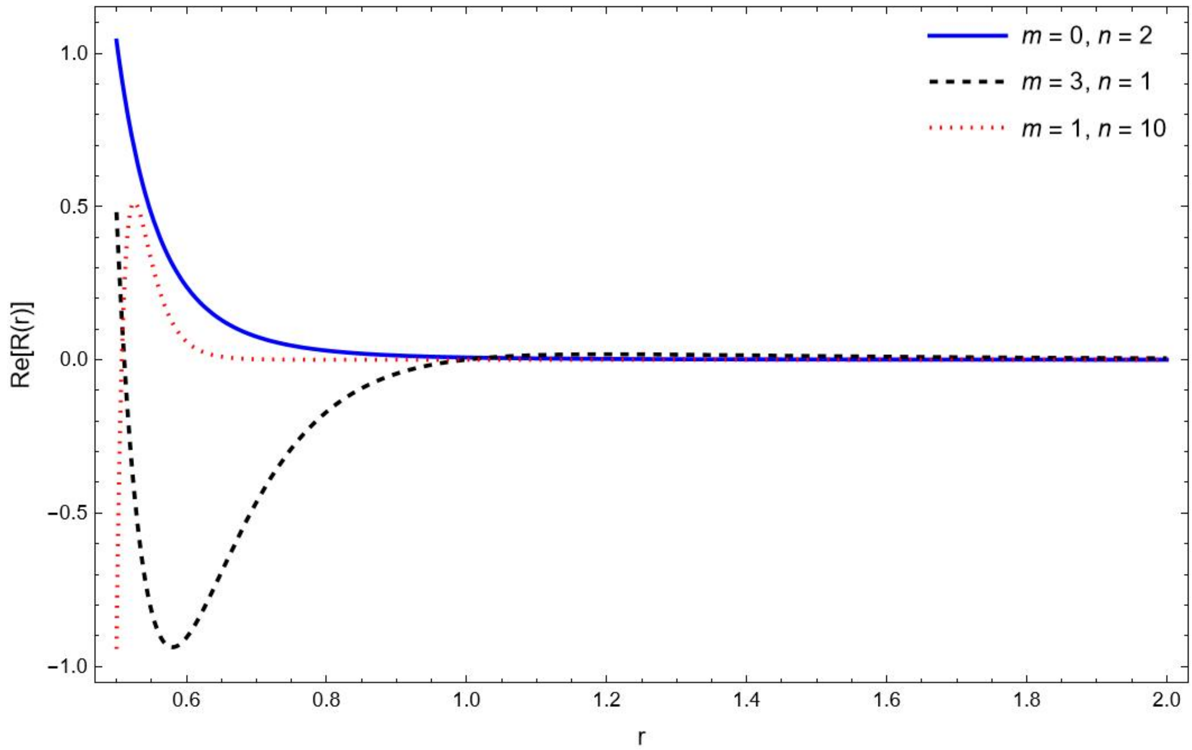

Figure 7: Plot of Re$[R(r)]$ from eqn. (27) for $(m, n) = (0, 2), (3, 1)$, and $(1, 10)$ with $r_+ = 1/2$ and $l = 1$. A factor of $c_1 = 1/120, 1/6$, and 5×10^{-5} were respectively chosen for visibility. Note that these solutions only hold for $r > r_+ = 1/2$. Furthermore, only the real portions of these functions are shown due to their physical relevance.

be non-negative integers n. Therefore, the quasinormal modes frequencies are:

$$\omega_n = \frac{m}{l} - \frac{2ir_+}{l^2}(n+1), \tag{38}$$

which matches the result in [22]. Figure 7 shows $R(r)$ for select values of m and n with $l = 1$ and $r_+ = 1/2$. Note that the quasinormal mode frequencies are consistent with eqn. (29) with $r_+ = il$. Finally, the quasinormal modes themselves are:

$$\varphi(x) = \mathrm{Re}\left(e^{-i\omega_n t}e^{im\phi}\left(1-\frac{r_+^2}{r^2}\right)^{-\frac{il^2\omega_n}{2r_+}} {}_2F_1\left(-\frac{i\omega_n l^2}{2r_+}-\frac{iml}{2r_+}, \frac{ilm}{2r_+}-\frac{i\omega_n l^2}{2r_+}; 1-\frac{i\omega_n l^2}{r_+}; 1-\frac{r_+^2}{r^2}\right)\right) \tag{39}$$

Note that the radial solution need not be real here; such a property only holds true for $m = 0$.

Throughout the derivation for both the AdS_3 and BTZ black hole spacetimes, the only constraints that were placed on the time parameters ω were the boundary conditions. Without them, ω was free to be any value. Of course, the physical dynamics of the setting is contained in the Klein-Gordon equation and the metric, but the boundary conditions were necessary to determine if the wavefunctions exhibit normal or quasinormal modes.

These examples show that deriving (quasi)normal modes of simple spacetimes interacting with the simplest field possible is not an easy process. As we shall see in the next section, analytical expressions for these values cannot be found even when adding one more spatial dimension.

3.3 Schwarzschild Black Hole

Here, the metric is

$$\mathrm{d}s^2 = -\left(\frac{r-2M}{r}\right)\mathrm{d}t^2 + \left(\frac{r}{r-2M}\right)\mathrm{d}r^2 + r^2\mathrm{d}\theta^2 + r^2\mathrm{sech}^2(x)\mathrm{d}\phi^2. \tag{40}$$

Solving the wave equation is straightforward, since the metric is diagonal using the above coordinates. By assuming $\varphi = R(r)T(t)g(\theta,\phi)$ and using separation of variables, we find that g is simply the spherical harmonics, which appear in other settings like the Hydrogen atom example in quantum mechanics. The time function is once again $T(t) = e^{-i\omega t}$, where ω are the quasinormal modes. Dividing these solutions out, we are left with the radial equation:

$$(r-2M)^2R''(r) = -\left(\frac{2(r-M)(r-2M)}{r}\right)R'(r) + \left(\frac{l(l+1)(r-2M)}{r} - \omega^2r^2\right)R(r), \tag{41}$$

where ω is the quasinormal mode frequencies and $l(l+1)$ is the separation constant for the angular terms. No solution exists for this equation, so there is no way to derive the quasinormal modes themselves. However, we can check if our radial equation has the correct limits as $r \to \infty$ and $r \to 2M$. This exercise will strengthen our understanding of the system.

3.3.1 Horizon Limit

In the latter limit, we can use the Frobenius method to determine if our solution has the appropriate limit as $r \to 2M$. First of all, it is easy to see that $r = 2M$ is a regular singular point of eqn. (41). Thus, the method is applicable here. Let $R = \sum_{k=0}^{\infty} A_k(r-2M)^{k+s}$. Then, we see that

$$0 = \sum_{k=0}^{\infty}\left[(k+s)(k+s-1) + \frac{2(r-M)}{r}(k+s) + \omega^2r^2\right]A_k(r_*)^{k+s} - \frac{l(l+1)}{r}\sum_{k=1}^{\infty}A_{k-1}(r_*)^{k+s}, \tag{42}$$

where $r_* = r - 2M$ was defined for convenience. The incident polynomial, which is the coefficient of A_0r^s, must be 0. Thus,

$$s = \frac{r_*}{2r} \pm \frac{1}{2}\sqrt{\frac{r_*^2}{r^2} - 4r^2\omega^2}. \tag{43}$$

To determine this sign, we need to employ the ingoing boundary condition at $r_* = 0$. When this value is plugged in, we find that $s = \pm 2iM\omega$. In addition, we see that under this limit:

$$R(r) \approx A_0(r_*)^{\pm 2i\omega M}. \tag{44}$$

The ingoing condition demands that $f(t,x) = Ce^{-i\omega(t+x)}$, where $x = r + 2M\ln(r_*)$ is the tortoise coordinate for a Schwarzschild metric. We already know that $e^{-i\omega t}$ is the solution to the ODE of time in eqn. (41), since the perturbation must be virtually nonexistent at a much later time. For r, note that $e^{-i\omega x} \propto r_*^{-2iM\omega}$, meaning that $s = -2iM\omega$.

All that is left for this direction is to find a recursion relation for A_k. The coefficient of z^{k+s} must vanish, so we have:

$$A_k = \frac{A_{k-1}}{Mk^2 - 4iM^2\omega k} \Longrightarrow A_k = \frac{c_1\,(M)^{1-k}}{(1)_{k-1}(1-4iM\omega)_{k-1}}, \tag{45}$$

where $(x)_k$ is the Pochhammer symbol. Thus, near the horizon, the radial solution is:

$$R(r) = A_0(r-2M)^{-2iM\omega} + c_1\sum_{k=1}^{\infty}\frac{(M)^{1-k}}{(1)_{k-1}(1-4iM\omega)_{k-1}}(r-2M)^{k-2iM\omega} \tag{46}$$

3.3.2 Far-field Limit

In the other limit, $r \to \infty$, our ODE becomes:

$$R''(r) + \frac{2}{r}R'(r) + \left(\omega^2 - \frac{l(l+1)}{r^2}\right) R(r) = 0. \tag{47}$$

The solution to this equation is:

$$R(r) = c_1 j_l(r\omega) + c_2 y_l(r\omega), \tag{48}$$

where j and y are the spherical Bessel functions of the first and second kinds respectively. Since our perturbation must vanish when r is very large, we can study the case where $\omega \ll 1$, since this reduces to the familiar Minkowski metric setting, and $r \gg 1$. Expanding the first solution, we get

$$j_l(r\omega) = C(r\omega)^{-1/2} J_{l+1/2}(r\omega) = C(r\omega)^{-1/2} \left(\sum_{m=0}^{\infty} \left(\frac{r\omega}{2}\right)^{2m+l+\frac{1}{2}} \right) \approx C\, r^l. \tag{49}$$

To make sure the second solution is the correct one, we can expand it too:

$$y_l(r\omega) = C(r\omega)^{-1/2} J_{-l-1/2}(r\omega) = C(r\omega)^{-1/2} \left(\sum_{m=0}^{\infty} \left(\frac{r\omega}{2}\right)^{2m-l-\frac{1}{2}} \right) \approx C\, r^{-(l+1)}. \tag{50}$$

Thus, $c_1 = 0$ in eqn. (48), meaning the radial equation in this regime is

$$R(r) = c_1 y_l(\omega r). \tag{51}$$

With a thorough review of the radial solution at the extreme limits done, we can now discuss how to find the quasinormal mode frequencies of this black hole.

3.3.3 Quasinormal Mode Frequencies of the Schwarzschild Black Hole

Since the radial equation cannot be solved, we will instead use perturbation theory instead of pure numerics to gain some perspective on ω. This work is based on the method described in [23].

Such a method is useful for its versatility; it can be used in a wide variety of situations, such as black holes with charge and spin [24, 25]. However, it possesses one major flaw: the series that it produces - that approximates the 'true' value of the sought-after parameter - is not always convergent. Thus, other methods such as the Borel summation or Padé approximants (see [26] for more detail) may be necessary.

A Quick Look at Perturbation Theory

To begin, let us rewrite the radial equation of this setting from eqn. (41) as

$$\left[f(z)\frac{d}{dz} f(z)\frac{d}{dz} + (2M\omega)^2 - f(z)\left(\frac{\ell(\ell+1)}{z^2} + \frac{1}{z^3}\right)\right] R(z) = 0, \tag{52}$$

where $z = r/2M$ and $f(z) = 1 - \frac{1}{z}$. Now, we can define the perturbation term as

$$\hbar = \sqrt{\frac{2}{\ell(\ell+1)}}. \tag{53}$$

Now, note that multiplying both sides by $\hbar^2$ allows us to write the previous equation as

$$\left(-\hbar^2 f(z)\frac{d}{dz}f(z)\frac{d}{dz}+V(z)^2\right)R(z)=ER(z), \tag{54}$$

where $E=(2\omega\hbar)^2$ is the energy term and $V(z)=V_0(z)+\hbar^2V_1(z)=f(z)\left(z^{-2}+\hbar^2z^{-3}\right)$ is the potential term. The ω term is the quasinormal mode frequencies that we are ultimately trying to find. It is easy to see that, to get this equation into a Schrodinger form, we go to the tortoise coordinate x defined by $x=z+\ln(z-1)+C$. We can strategically choose C such that V_0 reaches its maximum value at $x=0$. This corresponds to $z=3/2$, so $C=\ln(2)-3/2$. The advantage of doing so will be clear soon. We can now expand V_0 near its maximum:

$$\begin{aligned}
V_0(z)&=\frac{8}{27}-\frac{32}{729}\left(z-\frac{3}{2}\right)^2+O(z^3)\approx\frac{8}{27}-\frac{32}{729}x^2+O(x^3),\\
V_1(z)&=(1-s^2)\left(\frac{8}{81}-\frac{16}{729}x-\frac{32}{2187}x^2+O(x^3)\right),
\end{aligned} \tag{55}$$

where s is the spin weight of the background field. Now, we can do a couple of variable changes, $g=\sqrt{\hbar}$ and $q=x/g$, such that eqn. (54) becomes:

$$-\frac{1}{2}\psi''(q)+\frac{v(x)}{g^2}\psi(q)=\epsilon\psi(q), \tag{56}$$

where the function $v(x)$ is defined as follows:

$$v(x)=\frac{V_0(x)-V_0(0)}{2}+\frac{g^4(V_1(x)-V_1(0))}{2}=v_0(x)+g^4v_1(x). \tag{57}$$

Furthermore, $\epsilon=(E-V(0))/2g^2$. The actual perturbative expansion for the energy term is given by rewriting ϵ from the above equation into an infinite sum of a recursively defined variable $\epsilon_{n,l}$[9] and the perturbation term g:

$$E_n=(2\omega_n\hbar)^2=V(0)+2\hbar\left[\sum_{l=0}^{\infty}g^l\epsilon_{n,l}\right]=V(0)+2\hbar\left[-\sqrt{v_0''(0)}\left(n+\frac{1}{2}\right)+\sum_{l=1}^{\infty}g^l\epsilon_{n,l}\right]. \tag{58}$$

Note that $\sqrt{v_0''(0)}$ is not real. The inclusion of this imaginary number is what leads the mode frequencies to have a non-zero imaginary part. This is consistent with a field's perturbation exhibiting quasinormal mode frequencies in the presence of a black hole.

If we evaluate the terms $\epsilon_{n,l}$, then we can find ω_n in a straightforward manner. These terms are defined as:

$$\begin{aligned}
\epsilon_{n,0}&=-\sqrt{v_0''(0)}\left(n+\frac{1}{2}\right),\\
\epsilon_{n\geq 1,l}&=-\frac{(n+1)(n+2)}{2}A^{n+2}_{n,l}-\sum_{j=1}^{l-1}\epsilon_{n,j}A^n_{n,l-j}+\sum_{j=1}^{l}(v_{0,j}A^{n-j-2}_{n,l-j}+v_{1,j}A^{n-j}_{n,l-j-2}).
\end{aligned} \tag{59}$$

The symbols $A^k_{n,l}$ introduced in the above equation can be written as:

$$A^k_{n,l}=\begin{cases}
\frac{(k+1)(k+2)A^{k+2}_{n,l}+\sum_{j=1}^{l-1}2\epsilon_{n,j}A^k_{n,l-j}-2\sum_{j=1}^{l}(v_{0,j}A^{k-j-2}_{n,l-j}+v_{1,j}A^{k-j}_{n,l-j-2})}{2\sqrt{v_0''(0)}(k-n)} & n+1\leq k\leq n+3l\\
\frac{(k+1)(k+2)A^{k+2}_{n,l}+2\sum_{j=1}^{l}(\epsilon_{n,j}A^k_{n,l-j}-v_{0,j}A^{k-j-2}_{n,l-j}-v_{1,j}A^{k-j}_{n,l-j-2})}{2\sqrt{v_0''(0)}(k-n)} & 0\leq k\leq n-1\\
\delta_{0l} & k=n\\
0 & \text{otherwise}
\end{cases} \tag{60}$$

[9]The variables l and ℓ are different. We use this notation aware of this clash in order to match the notation of [23], which this section is based on.

Here, $v_{0,j} = \frac{v_0^{(j+2)}(0)}{(j+2)!}$[10] and $v_{1,j} = \frac{v_1^{(j)}(0)}{j!}$. Since perturbation theory is not a main focus of this report, we introduced and defined new terms without much of a derivation. A technical review of this method can be found in [27, 28].

An Illustrative Example

To showcase the perturbative method described above, let us find the quasinormal mode frequencies for a set of n, l, and s values. To rederive the work in [23], we choose $n = 0$, $\ell = 2$, and $s = 2$. Firstly, eqns. (59) and (60) state that:

$$\epsilon_{0,l} = A^2_{0,l}. \tag{61}$$

Finding these symbols is enough to get a perturbative expansion for the quasinormal modes. Since the first equation of eqn. (60), which is the most relevant for this choice of parameters, is an implicit recursive relation, it is necessary to find $A^{3l}_{0,l} \cdots A^3_{0,l}$ before $A^2_{0,l}$. This can be done in a straightforward manner, as $A^k_{n,l}$ with k or l being negative vanish.

Rewriting eqn. (58) up to order $\hbar^3$, we can finally find the quasinormal mode frequencies:

$$\omega_n\Big|_{n=0,l=2,s=2} = \sqrt{\frac{3}{4}\left[\frac{8}{27} - \frac{4i}{27}\hbar - \frac{281}{729}\hbar^2 + \frac{6163i}{26244\sqrt{2}}\hbar^3 + \mathcal{O}(\hbar^4)\right]} = 0.36628 - 0.0911245i. \tag{62}$$

Since eqn. (58) contains powers of $g = \sqrt{\hbar}$ rather than $\hbar$, one might expect fractional powers of $\hbar$ in the expression for ω_n. However, the recursion relation for the $A^k_{n,l}$ symbols dictate that $A^2_{0,l} = 0$ for odd l. In addition, the positive square root was chosen above to make sure $\mathrm{Im}(\omega_n)$ is negative by definition.

The result above is consistent with the findings of [23]. The frequencies themselves are correct up to order 10^{-2} with both the perturbative and numerical approximations performed in the same paper. Their work also showcases how the difference between the types of approximations is of order 10^{-5} when terms up to $\hbar^{12}$ are considered in eqn. (62). In addition, the approximation will get stronger for higher values of ℓ, since the perturbative parameter $\hbar$ grows smaller.

This exercise, along with the 2 + 1 dimensional examples, provide a brief glimpse into the derivation of (quasi)normal modes, which are complex even in the simplest settings. The methods presented above are not the only ways to find these modes, however. In fact, the bootstrap method can be easily applied here, even though this is not a quantum system. As an example, we return to the BTZ black hole. We shall bootstrap this setting and discuss some problems we come across.

3.4 Bootstrapping the BTZ Black Hole

Recall that there is nothing intrinsically quantum mechanical about bootstrapping. Of course, the equations that have been numerically investigated thus far have been the Schrodinger's equation, but any differential equation of the form in eqn. (1) is fair game. Thus, if we can convert the radial equation from eqn. (33) to such a form, then the bootstrap method can be implemented.

Fortunately, this process is simple. This can be done with a change of coordinates to the all-too-familiar tortoise coordinates. To make the mathematics simpler, we define $x = \frac{1}{2}\log\left(\frac{r-r_+}{r+r_+}\right)$,

[10]This formula is written incorrectly in [23] as $v_{0,j} = \frac{v_0^{(j)}(0)}{j!}$. The correct form that we have written comes from [27]

where we assume $l = 1$ and absorb the r_+ in the denominator with the x for simplicity. We first rescale our differential equation by $R(r) \to R(r)/\sqrt{r}$ ans then apply the coordinate change. Finally, we substitute in eqn. (38) for ω_n, so our equation becomes

$$-\frac{u''(x)}{2} + \left(\frac{3}{8}\text{csch}^2(x) + \frac{1}{8}\text{sech}^2(x)\right) u(x) = -2(n+1)^2 u(x). \tag{63}$$

Note that we set $m = 0$ to first test the bootstrap method for the simplest setting. In addition, a factor of $1/2$ was introduced to match the form of the Schrodinger's equation. Thus, our potential is $V(x) = \frac{3}{8}\text{csch}^2(x) + \frac{1}{8}\text{sech}^2(x)$. Such a potential is reminiscent of the Pöschl-Teller potential; the inclusion of the hyperbolic cosecant term makes it a more general Pöschl-Teller potential.

The next step is to determine the operator needed for the moment sequence. An immediate thought might be a linear combination of $\text{csch}(x)$ and $\text{sech}(x)$. However, attempting to do so fails as their coefficients are not identical. Another approach is using e^x, since all hyperbolic functions special forms of the exponential. Such a sequence is possible, but this becomes too complicated due to the many exponential functions in the denominator; this makes the search space large. In fact, the easiest moment operator to consider $\text{sech}(x)$, the exact same one as Section 2.2. The derivation of the recursion relation is slightly trickier, however.

The operators used in the bootstrap constraints have to be chosen carefully. Naively using the same operators as Section 2.2 yields terms with $\text{csch}(x)$, which cannot be rid. To counteract these, we include factors of $\sinh(x)$. An easy conversion exists between even powers of $\sinh(x)$ and $\text{sech}(x)$ through the Pythagorean theorem, and the remaining $\sinh(x)$ terms gets substituted out for another identity.

First, let us consider $\mathcal{O} = \text{sech}^n(x)\sinh^3(x)p$ in the commutator constraint of bootstrap, where the $\sinh^3(x)$ was included to cancel out the hyperbolic cosecant term in $V'(x)$. Using a more general potential of $V(x) = a\text{csch}^2(x) + b\text{sech}^2(x)$, we find:

$$-\frac{1}{2}\alpha = i\beta - i\gamma, \tag{64}$$

where

$$\begin{aligned}
\alpha =& (3-n)\left(\langle\text{sech}^{n-3}(x)p^2\rangle - \langle\text{sech}^{n-1}(x)p^2\rangle\right) + n\left(\langle\text{sech}^{n-1}(x)p^2\rangle - \langle\text{sech}^{n+1}(x)p^2\rangle\right), && \text{(65a)}\\
\beta =& (n-3)^2\langle\text{sech}^{n-2}(x)\sinh(x)p\rangle - (2n-3)(n-1)\langle\text{sech}^{n}(x)\sinh(x)p\rangle && \text{(65b)}\\
&+ n(n+1)\langle\text{sech}^{n+2}(x)\sinh(x)p\rangle,\\
\gamma =& -2(a+b)\langle\text{sech}^{n-1}(x)\rangle + 4b\langle\text{sech}^{n+1}(x)\rangle - 2b\langle\text{sech}^{n+3}(x)\rangle. && \text{(65c)}
\end{aligned}$$

Thus, all we need to do is substitute out $\langle\text{sech}^m(x)\sinh(x)p\rangle$ and $\langle\text{sech}^m(x)p^2\rangle$. We have already found a relation for the former term; the first equation in eqn. (10), which was one of the relations found in the Pöschl-Teller potential, applies here as well. The latter term is also straightforward to substitute out. Plugging in $\mathcal{O} = \text{sech}^m(x)\sinh^2(x)$ into the constraint with the energy term, we find

$$\langle\text{sech}^{m-2}(x)p^2\rangle - \langle\text{sech}^{m}(x)p^2\rangle = 2\left(E\langle\text{sech}^{m-2}(x)\rangle - (E+a+b)\langle\text{sech}^{m}(x)\rangle + b\langle\text{sech}^{m+2}(x)\rangle\right). \tag{66}$$

There may be concern that the above linear combination of $\text{sech}^{m-2}(x)p^2$ is not present in eqn. (64). However, this exact linear combination is found, so the above relation can be used without caution. Thus, with $a = 3/8$ and $b = 1/8$, a recursion relation can be found for the BTZ black hole:

$$r_n = -\frac{c_1 r_{n-1} + c_2 r_{n-2} + c_3 r_{n-3}}{-2n^3 + 6n^2 - 6n + 2}, \tag{67}$$

where $r_n = \langle \text{sech}^n(x) \rangle$ and

$$\begin{aligned} c_1 &= \left(4En - 6E + 6n^3 - 30n^2 + 54n - 34\right), \\ c_2 &= \left(-8En + 18E - 6n^3 + 42n^2 - 102n + 86\right), \\ c_3 &= \left(4En - 12E + 2n^3 - 18n^2 + 54n - 54\right). \end{aligned} \tag{68}$$

It is easy to see that we rescaled the exponents such that the our moment sequence is now $\{r_n\}_{n=0}^{\infty}$, where $r_n = \langle \text{sech}^{2n}(x) \rangle$. In addition, note that the search space for this problem contains three elements: E, $\langle \text{sech}^2(x) \rangle$, $\langle \text{sech}^4(x) \rangle$. Thus, our search space is three-dimensional, just like the setting in Section 2.3.3.

3.5 Issues with the Wavefunction of the BTZ Black Hole

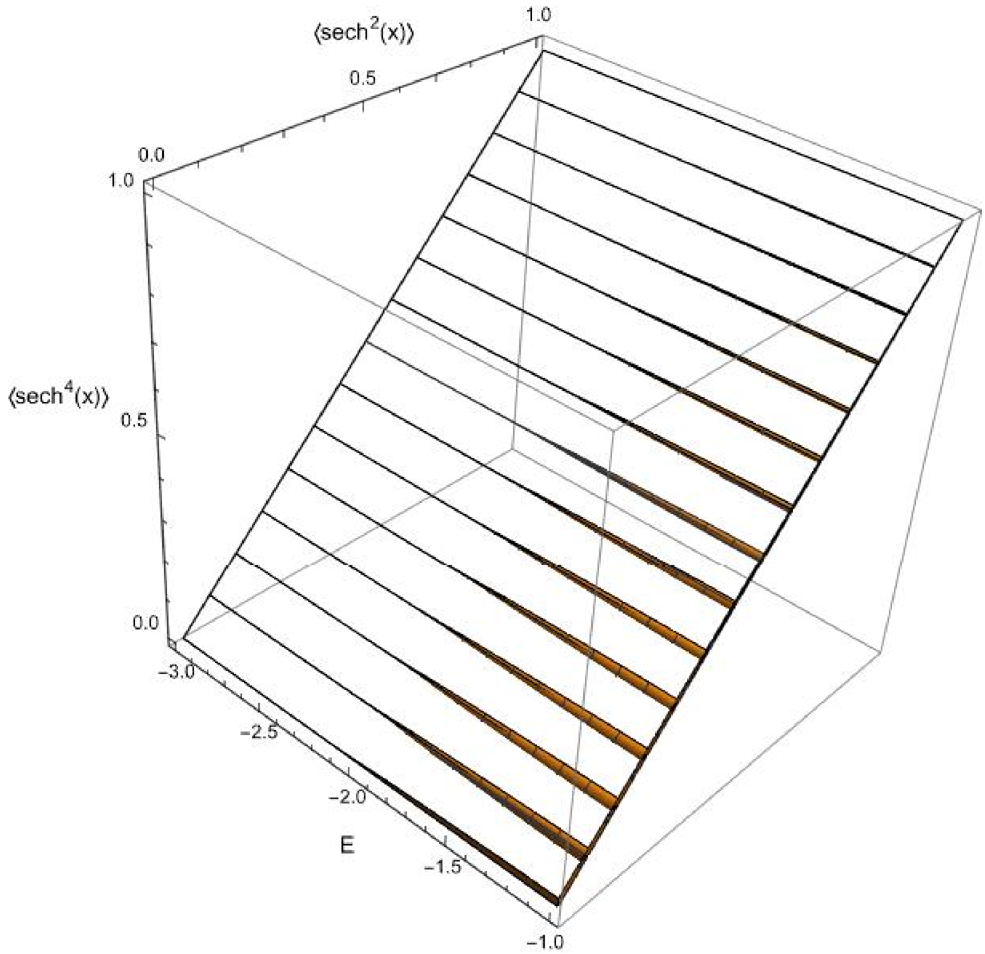

Figure 8: Plot of the allowed regions of E, $\langle \text{sech}^2(x) \rangle$, and $\langle \text{sech}^4(x) \rangle$ found through the positivity constraint. In this scenario, the positivity constraint included negative eigenvalues of order -10^{-6} to mitigate numerical noise. This plot is reminiscent of the plane $\langle \text{sech}^2(x) \rangle = \langle \text{sech}^4(x) \rangle$.

With the recursion relation having been derived, we can proceed with using the bootstrap method, the result of which can be found in Figure 8. It is important to mention that this setting produced a high amount of numerical noise that we did not come across in other situations. That is, there were regions of the search space where the smallest eigenvalue was negative of order 10^{-15}. It is a reasonable assumption that these values are 0, so to account for these points, we slightly modified the positivity constraint. Rather than all eigenvalues having to be non-negative, we demand that they have to be greater than -10^{-6}. The graph in Figure 8 follows this principle as well.

This graph shows that the bootstrap method finds the $E = -2$ quasinormal mode. However, there is no distinction between the $E = -2$ and $E = -2.5$ energy values. In fact, when zoomed out, the general planar shape of allowed eigenvalues can be found for all values of E. More specifically, this plane appears where $\langle \mathrm{sech}^2(x)\rangle = \langle \mathrm{sech}^4(x)\rangle$. This plane seems to satisfy the positivity constraint for various values of K, meaning that the bootstrap method is not successful here in determining the quasinormal modes[11].

To gain a better understanding of this counter-intuitive result, we turned to finding the expectation values of $\mathrm{sech}^2(x)$ and $\mathrm{sech}^4(x)$ analytically. The radial equation, which is the wave function here, has already been found in Section 3.2. It is straightforward to convert this to the modified tortoise coordinates. However, we arrive at a new problem: $\langle \mathrm{sech}^2(x)\rangle$ and $\langle \mathrm{sech}^4(x)\rangle$ diverge. In fact, this wave function isn't normalizable, since $\langle 1\rangle$ also diverges. This fact should not be too surprising, given the shape of the potential. It is easy to see that the potential approaches 0 as $x \to -\infty$, which explains the divergence.

However, it is still surprising that such a potential appears when converting the BTZ radial equation to a Schrodinger-like equation, since the quasinormal modes were retrievable in the gravity approach. This issue is more fundamental, and may be traced back to the metric. Figure 9 contains a Penrose diagram of the black hole. The path we are taking here, as per the metric from eqn. (31), is the red arrow in the diagram. This intersects with a point that is present in both the black and white holes' event horizon. Taking a different path in this geometry may resolve this issue. One such metric is the following:

$$\mathrm{d}s^2 = 2\mathrm{d}v\mathrm{d}r - \left(\frac{r^2 - r_+^2}{l^2}\right)\mathrm{d}v^2 + r^2\mathrm{d}\phi^2, \tag{69}$$

which corresponds to the blue path of the Penrose diagram. Here, $v = t + x$. We are in the process of determining if this method can resolve the issue of normalization.

While we have not fully solved this problem, the above work provides some insight on how to view a gravitational problem as a quantum mechanical one. Deriving a recursion relation with a complex potential shows the bootstrap in action for a richer setting. These examples are illustrative of the versatility of the bootstrap method. In the next section, we move on to applying this method to matrix models.

4. Matrix Quantum Mechanics

In matrix models, the Hamiltonian is a function of the trace of P and X, which are now $N \times N$ Hermitian matrices such that $[P_{ij}, X_{kl}] = -i\delta_{il}\delta_{jk}$. Like before, we have the bootstrap constraint from eqn. (2a), where $\langle \mathcal{O}\rangle = \mathrm{Tr}\,(\rho\mathcal{O})$ and ρ is the density matrix corresponding to an energy eigenstate or mixed thermal state. In addition, physical states in gauged matrix models must satisfy $\langle \mathrm{Tr}(G\mathcal{O})\rangle = 0$, where

$$G = i[X, P] + NI. \tag{70}$$

These are the generators of $SU(N)$. If the system was rotationally invariant with generators S, then we would have $\langle [S, \mathcal{O}]\rangle = 0$. The examples below will not use this symmetry, but one case can be found in [29]. In addition, we may use the cyclicity of the trace at large N to derive relations between two operators, such as $\langle \mathrm{Tr}(XP)\rangle$ and $\langle \mathrm{Tr}(PX)\rangle$, for example[12]. Finally, we

[11]No region other than the plane in the search space satisfies the positivity constraint, so we only observed this plane for various K

[12]The term $\langle \mathrm{Tr}(XP)\rangle$ contains two traces by the definition of $\langle \cdots \rangle$ here. While this seems redundant, such notation makes it clear that we are working with energy eigenstates/mixed thermal states. This is especially important in settings where N is not large; operators other than simple trace operators need to be considered there.

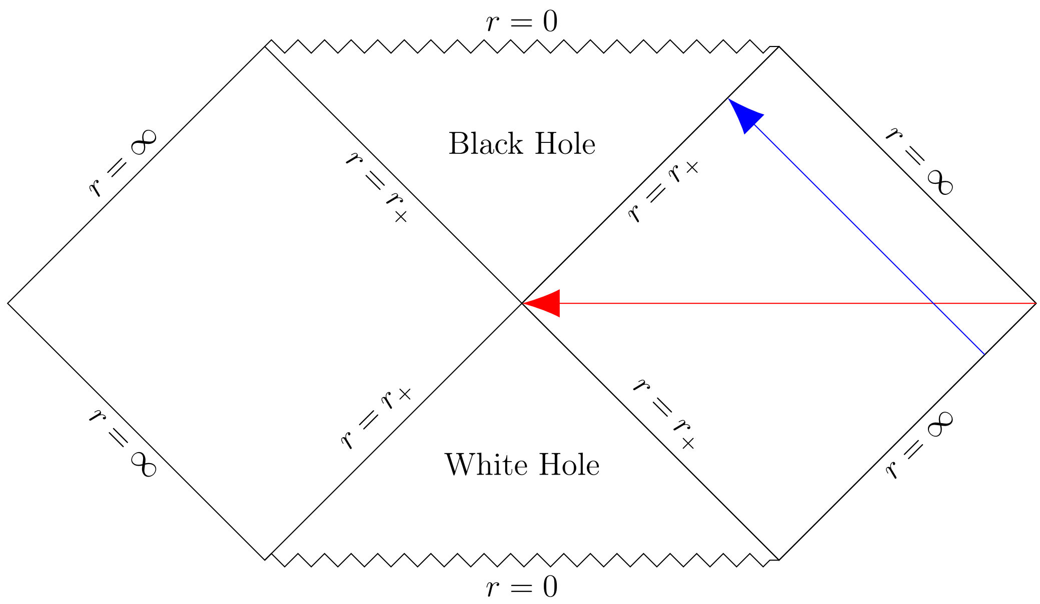

Figure 9: Penrose diagram of the BTZ geometry. The path that leads to a wave function that cannot be normalized, which is a product of the metric from eqn. (31), is depicted by the red, horizontal arrow. This path extends to the point of the event horizon that is shared by both the white and black holes. Avoiding this point may be the key to resolving this issue. One such way to do so is the blue, slanted path.

have that $\langle \mathcal{O}^\dagger \rangle = \langle \mathcal{O} \rangle^*$. To summarize, we have the following constraints for bootstrapping matrix models:

$$\begin{aligned}
\langle [H, \mathcal{O}] \rangle &= 0, && \text{(Commutator Constraint)} \\
\langle \mathrm{Tr}(G\mathcal{O}) \rangle &= 0, && \text{(Symmetry Constraint)} \\
[A, B_1 B_2 \cdots B_n] &= \sum_{i=1}^{n} c_i \mathrm{Tr}\left(B_1 \cdots B_{i-1}\right) \mathrm{Tr}\left(B_{i+1} \cdots B_n\right), && \text{(Cyclicity of Trace)} \\
\langle \mathcal{O}^\dagger \rangle &= \langle \mathcal{O} \rangle^* && \text{(Conjugate Constraint)}
\end{aligned}$$

The positivity constraint is also present here, but it is slightly different than the single particle case. Our goal is to create a matrix like Table 1. It is easy to see that this matrix and all of its submatrices satisfy the positivity constraint from eqn. (3); all of these submatrices, whether they are connected or not, must have a non-negative determinant. The row and column headers are not included as elements of the matrix, and they are only included to provide structure for the matrix. The constraint grows stronger as we utilize more operators. As a metric for the number of operators, we shall consider lengths of strings. That is, all operators with some length up to L will be used in the row and column headers. For example, for $L = 2$ in single matrix quantum mechanics, we place the operators $\{I, X, P, X^2, P^2, XP, PX\}$ in the headers, so our matrix would consist of 49 elements. In general, there are $2^{L+1} - 1$ operators with length less than or equal to L. Accounting for all of the submatrices, we get $2^{2^{L+1}-1} - 1$ determinant constraints. For $L = 5$, this number is of order 10^{18}, meaning that bootstrapping should be limited to low values of L.

The aim of applying bootstrap to matrix models is to construct such a matrix and simplify its elements using the constraints mentioned prior. There will be parameters that cannot be reduced, and we can find a lower bound of energy by minimizing $\langle H \rangle$ with respect to these parameters. Before we enter the D0-Brane Matrix Model, let us take a look at a simple example.

	I	$\mathcal{O}_1$	$\cdots$	$\mathcal{O}_n$
I	N	$\langle \mathrm{Tr}(\mathcal{O}_1) \rangle$	$\cdots$	$\langle \mathrm{Tr}(\mathcal{O}_n) \rangle$
$\mathcal{O}_1$	$\langle \mathrm{Tr}(\mathcal{O}_1^\dagger) \rangle$	$\langle \mathrm{Tr}(\mathcal{O}_1 \mathcal{O}_1^\dagger) \rangle$	$\cdots$	$\langle \mathrm{Tr}(\mathcal{O}_n \mathcal{O}_1^\dagger) \rangle$
$\vdots$	$\vdots$	$\vdots$	$\ddots$	$\vdots$
$\mathcal{O}_n$	$\langle \mathrm{Tr}(\mathcal{O}_n^\dagger) \rangle$	$\langle \mathrm{Tr}(\mathcal{O}_1 \mathcal{O}_n^\dagger) \rangle$	$\cdots$	$\langle \mathrm{Tr}(\mathcal{O}_n \mathcal{O}_n^\dagger) \rangle$

Table 1: A general table/matrix used in bootstrapping matrix models. It is easy to see that this matrix is Hermitian, making it compatible with the positivity constraint. This constraint states that all possible submatrices of this matrix must be positive semi-definite.

4.1 Anharmonic Oscillator

We begin with the anharmonic oscillator, which is an example that has already been bootstrapped [29]. The Hamiltonian of this model is

$$H = \mathrm{Tr}\left(P^2\right) + \mathrm{Tr}\left(X^2\right) + \frac{g}{N}\mathrm{Tr}\left(X^4\right). \tag{72}$$

Let us first construct a matrix using strings with length 1 and under. Thus, the headers will consist of I, X, P. Since the Hamiltonian is quadratic, we must have $\langle \mathrm{Tr}(X) \rangle = \langle \mathrm{Tr}(P) \rangle = 0$. Therefore, the only unknown, non-vanishing elements of the matrix are $\langle \mathrm{Tr}(X^2) \rangle$, $\langle \mathrm{Tr}(P^2) \rangle$, $\langle \mathrm{Tr}(PX) \rangle$, and $\langle \mathrm{Tr}(XP) \rangle$. The latter are easy to solve for. Using $\langle \mathrm{Tr}(G) \rangle = 0$, we find that

$$\langle \mathrm{Tr}(XP) \rangle = -\langle \mathrm{Tr}(PX) \rangle = \frac{iN^2}{2} \tag{73}$$

In addition, $[H, \langle \mathrm{Tr}(X^2) \rangle]$ gives us

$$\langle \mathrm{Tr}(P^2) \rangle = \langle \mathrm{Tr}(X^2) \rangle + \frac{2g}{N}\langle \mathrm{Tr}(X^4) \rangle \tag{74}$$

The other two elements cannot be found given our constraints, so $\langle \mathrm{Tr}(X^2) \rangle$ and $\langle \mathrm{Tr}(X^4) \rangle$ are the parameters used to minimize $\langle H \rangle = 0$. The matrix for this calculation can be found in Table 2. We used `FindMinimum` to do so, resulting in the lower bound found in Figure 10. It is clear that this lower bound is not strict enough to understand the system. Thus, we move onto the $L = 2$ case.

	I	X	P
I	N	0	0
X	0	$\langle \mathrm{Tr}(X^2) \rangle$	$-i\frac{N^2}{2}$
P	0	$i\frac{N^2}{2}$	$\langle \mathrm{Tr}(X^2) \rangle + \frac{2g}{N}\langle \mathrm{Tr}(X^4) \rangle$

Table 2: Bootstrap matrix using all strings with length ≤ 1.

As mentioned prior, our list of strings to use becomes $\{I, X, P, X^2, P^2, XP, PX, \}$. Table 3 contains the $L = 2$ matrix. More information about the simplification of this matrix using the bootstrap constraints can be found in Appendix A. From this matrix, we see that there are four unknown parameters in this case, meaning that the minimization problem becomes much more complex in this setting. The lower bound for E can be found in Figure 10. This is much closer than the $L = 1$ lower bound to the exact energy ground state energy value, which can be analytically found through mapping this problem to one of N free fermions [30]. It is worth mentioning that this lower bound is not the exact one that was found in [29] for the $L = 2$ case, which was done in Python. This is most likely due to the minimization algorithms themselves.

This example serves as a decent introduction to applying the bootstrap method to matrix models. Using this knowledge, we can begin bootstrapping the D0-Brane Matrix Model.

	I	X^2	P^2	XP	PX	X	P
I	N	a	$a+\frac{2g}{N}b$	$\frac{iN^2}{2}$	$-\frac{iN^2}{2}$		
X^2	a	b	d	0	$-iNa$		
P^2	$a+\frac{2g}{N}b$	d	c	$iNa+\frac{2ig}{N}b$	0		
PX	$-\frac{iN^2}{2}$	0	$-iNa-\frac{2ig}{N}b$	$d+\frac{n^3}{2}$	d		
XP	$\frac{iN^2}{2}$	iNa	0	d	$d+\frac{n^3}{2}$		
X						a	-$\frac{iN^2}{2}$
P						$\frac{iN^2}{2}$	$a+\frac{2g}{N}b$

Table 3: Bootstrap matrix using strings of length ≤ 2, where the empty elements are zeroes. Here. $a = \langle \mathrm{Tr}(X^2)\rangle, b = \langle \mathrm{Tr}(X^4)\rangle, c = \langle \mathrm{Tr}(P^4)\rangle$, and $d = \langle \mathrm{Tr}(XPXP)\rangle$. Note that there are 49 elements, meaning that there are $2^7 - 1 = 127$ submatrices and determinant constraints.

4.2 D0-Brane Matrix Model

It is important to note that the following discussion on and our understanding of the D0-Brane Matrix Model comes from Lin's paper [11]. As such, our work will follow Lin's work, and we shall rederive his results.

Before we can do so, we must understand the various components of the Hamiltonian, which is

$$H = \frac{1}{2}\mathrm{Tr}\left(\sum_{I,J}\left(g^2 P_I^2 - \frac{1}{2g^2}[X_I, X_J]^2 - \psi_\alpha \gamma^I_{\alpha\beta}[X_I, \psi_\beta]\right)\right). \tag{75}$$

Here, X_I are the 9 bosonic matrices and ψ_α are the 16 fermionic matrices present in this theory such that $\{\psi_{ij}, \psi_{kl}\} = [X_{ij}, X_{kl}] = \delta_{il}\delta_{jk}$. All of these matrices are traceless and Hermitian, like in the anharmonic oscillator setting. Furthermore, γ^I are the gamma matrices of SO(9) such that $\{\gamma^I, \gamma^J\} = 2\delta^{IJ}$. We are interested in studying this problem in the so called *'t Hooft limit*, in which this system transforms into a 10 dimensional black hole of string theory with the metric:

$$\frac{\mathrm{d}s^2}{\alpha'} = -f(r) r_c^2 \mathrm{d}t^2 + \frac{\mathrm{d}r^2}{f(r) r_c^2} + \left(\frac{r}{r_c}\right)^{-3/2} \mathrm{d}\Omega_8^2, \tag{76}$$

where

$$\begin{gathered} f(r) = \left(1 - \frac{r_h^2}{r^2}\right)\left(\frac{r}{r_c}\right)^{7/2}, \\ r_c = \sqrt[3]{240\pi^5 g^2 N}. \end{gathered} \tag{77}$$

This limit is found when keeping the dimensionless quantity $\lambda/T^3 = g^2 N/T^3$ fixed as $N \to \infty$. More information about this and other limits of this model can be found here [31, 32].

In this report, we will not be working with the gravitational side of this problem. Our goal is to determine constraints on the energy and observables of the system, such as $\langle X^n\rangle$ for some arbitrary n, from the matrix model perspective[13]. The general strategy to do so is to construct lower bounds from the bosonic and the fermionic terms. Then, we can combine contributions from both to create a stronger constraint. To do so efficiently, we rewrite the Hamiltonian in the following manner:

$$H = \mathcal{K} + \mathcal{B} + \mathcal{F}, \tag{78}$$

where $\mathcal{K}, \mathcal{B}$, and $\mathcal{F}$ are the kinetic, bosonic, and fermionic terms of eqn. (75) respectively.

[13] There has been discussion about what these observables represent in the gravitational side [33].

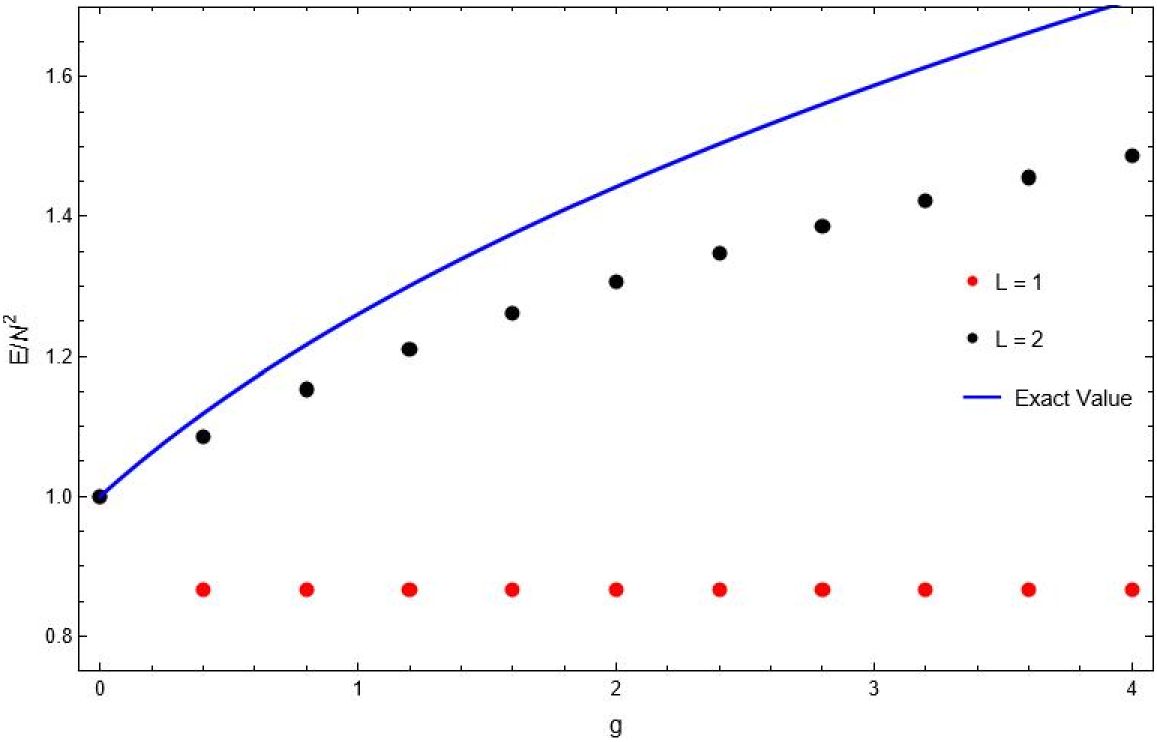

Figure 10: Plot of the lower bounds of the ground state energy along with the exact value (orange, smooth) as a function of g. These lower bounds are from the positivity constraints of the bootstrap matrices corresponding to $L = 1$ (blue, lower) and $L = 2$ (purple, higher).

4.2.1 Bosonic Contribution

To derive a constraint from the bosonic terms, we must eliminate the fermionic terms. This is straightforward; using $\langle H, \langle \mathrm{Tr}(XP)\rangle\rangle = 0$, we find

$$-2\langle\mathcal{K}\rangle + 4\langle\mathcal{B}\rangle + \langle\mathcal{F}\rangle = 0. \tag{79}$$

Combining this with $\langle H\rangle = E$, we find that

$$-\langle\mathcal{K}\rangle + \langle\mathcal{B}\rangle + \frac{1}{3}E = 0. \tag{80}$$

Now, let us take a closer look at $\mathcal{B}$. Let A, B be arbitrary bosonic matrices. Then, the Cauchy-Schwarz inequality states that

$$\langle \mathrm{Tr}(A^2)\rangle^2 \langle \mathrm{Tr}(B)\rangle^2 \geq \langle \mathrm{Tr}(AB)\rangle^2 \geq 0. \tag{81}$$

The term on the left is 0 by definition of the bosonic matrices, meaning $\langle \mathrm{Tr}(AB)\rangle = 0$. Thus, we may write $[A, B]^2$ in the following way:

$$[A, B]^2 = ABAB + BABA - AB^2A - BA^2B = 2ABAB - 2A^2B^2, \tag{82}$$

where the cyclicity of the trace is used. More specifically, we find that $A^2B^2 - AB^2A$ and $B^2A^2 - BA^2B$ are proportional to $\langle \mathrm{Tr}(AB)\rangle$, which we showed was 0. In addition, we combined terms using the conjugate constraint. We are then able to use the positivity constraint to simplify the bosonic term. With the matrices seen in Tables 4 and 5, we find the following constraints:

$$\begin{aligned} \langle \mathrm{Tr}(A^4)\rangle\langle \mathrm{Tr}(B^4)\rangle &\geq \langle \mathrm{Tr}(A^2B^2)\rangle^2, \\ \langle \mathrm{Tr}(A^2B^2)\rangle^2 &\geq \langle \mathrm{Tr}(ABAB)\rangle^2. \end{aligned} \tag{83}$$

The symmetry of the situation demands that $\langle \mathrm{Tr}(A^4)\rangle \geq \langle \mathrm{Tr}(A^2B^2)\rangle \geq \langle \mathrm{Tr}(ABAB)\rangle$. Then, with eqn. (82), we find

$$4g^2\langle \mathcal{B}\rangle = -\sum_{I,J}^{9}\langle \mathrm{Tr}([X_I, X_J]^2)\rangle \leq 72(2\langle \mathrm{Tr}(X^4)\rangle + 2\langle \mathrm{Tr}(X^4)\rangle) = 288\langle \mathrm{Tr}(X^4)\rangle, \tag{84}$$

where X is an arbitrary bosonic matrix.

	A^2	B^2
A^2	$\langle \mathrm{Tr}(A^4)\rangle$	$\langle \mathrm{Tr}(A^2B^2)\rangle$
B^2	$\langle \mathrm{Tr}(A^2B^2)\rangle$	$\langle \mathrm{Tr}(B^4)\rangle$

Table 4: Bootstrap matrix used to determine $\langle \mathrm{Tr}(A^4)\rangle \geq \langle \mathrm{Tr}(A^2B^2)\rangle$.

	AB	BA
AB	$\langle \mathrm{Tr}(A^2B^2)\rangle$	$\langle \mathrm{Tr}(ABAB)\rangle$
BA	$\langle \mathrm{Tr}(ABAB)\rangle$	$\langle \mathrm{Tr}(A^2B^2)\rangle$

Table 5: Bootstrap matrix used to determine $\langle \mathrm{Tr}(A^2B^2)\rangle \geq \langle \mathrm{Tr}(ABAB)\rangle$.

To utilize this fact, we turn to a constraint used in Section 4.1: for the $L = 1$ case, it is straightforward to see that $\langle \mathrm{Tr}(X^2)\rangle\langle \mathrm{Tr}(P^2)\rangle \geq \langle \mathrm{Tr}(XP)\rangle\langle \mathrm{Tr}(PX)\rangle = N^4/4$. In fact, this relation holds true here, since $\langle \mathrm{Tr}(XP)\rangle$ and $\langle \mathrm{Tr}(PX)\rangle$ retain their value in this setting. However, we have multiple X and P matrices here. Keeping the same X as used in the above calculations, it is easy to see that

$$\sum_I \langle \mathrm{Tr}(X^2)\rangle\langle \mathrm{Tr}(P_I^2)\rangle = \frac{2}{g^2}\langle \mathrm{Tr}(X^2)\rangle\langle \mathcal{K}\rangle \geq \frac{9}{4}N^4. \tag{85}$$

Thus, using eqns. (80), (84), and (85), we find the following constraint on E and $\langle \mathrm{Tr}(X^4)\rangle$:

$$\sqrt{\langle \mathrm{tr}(\tilde{X}^4)\rangle}\left(144\langle \mathrm{tr}(\tilde{X}^4)\rangle + \frac{2}{3}\varepsilon\right) \geq \frac{9}{4}, \tag{86}$$

where $\varepsilon = \lambda^{-1/3}N^{-2}E$, $\tilde{X} = \lambda^{-1/3}X$, and $\langle \mathrm{tr}(\cdots)\rangle = \langle \mathrm{Tr}(\cdots)\rangle/N$. A couple of important points to note here. Firstly, we used the constraint $N\langle \mathrm{Tr}(X^4)\rangle \geq \langle \mathrm{Tr}(X^2)\rangle^2$, which is trivial to find from the positivity constraint. In addition, we have changed notation to match our work with [11]. The reason this notation is used is to rid our constraint of the N dependence. This allows for us to study the system at arbitrary N.

The relationship between the energy ε and $\langle \mathrm{tr}(\tilde{X}^4)\rangle$ can be found in Figure 11. The plot shows that the bosonic terms provide a better lower bound for $\langle \mathrm{tr}(\tilde{X}^4)\rangle$ for lower energies. More specifically, these correspond to $\varepsilon \ll 1$ and $\varepsilon \gg 1$ respectively. Such an analysis is quite surprising from a simple bootstrap constraint such as this one, since $\varepsilon \sim 1$ is when the super-gravity solution begins to be invalid [11].

To find a stronger bound for high energies, we must turn towards fermions.

4.2.2 Fermionic Contribution

Working with the fermionic terms is more challenging. To effectively apply the positivity constraint on these terms, we rewrite $\mathcal{F}$ into $\sum_I\langle \mathrm{Tr}(O_I X_I)\rangle$. The explicit form of O_I will not be relevant for us, but we can find relations of O_I. The derivations for these require a better understanding of Majorana fermions and the generators of $\mathfrak{su}(N)$, which is the Lie algebra of $\mathrm{SU}(N)$. As such, we shall not provide these in this report, but they can be found in [11].

Firstly, using $\langle [H, \mathcal{F}]\rangle = 0$, we find that $\sum_I\langle \mathrm{Tr}(O_I P_I)\rangle = 0$. In addition, it can be shown that $\langle \mathrm{Tr}(O^2)\rangle \leq 64N^3$, where O is an arbitrary element of $\{O_I\}$. We can then construct a matrix to bootstrap, which can be found in Table 6. The positivity constraint then yields:

$$\langle \mathrm{tr}(\tilde{X}^2)\rangle \geq \frac{\left(\frac{\varepsilon}{9} - \frac{b}{3}\right)^2}{144} + \frac{3}{8\left(\frac{\varepsilon}{9} + \frac{b}{3}\right)}, \tag{87}$$

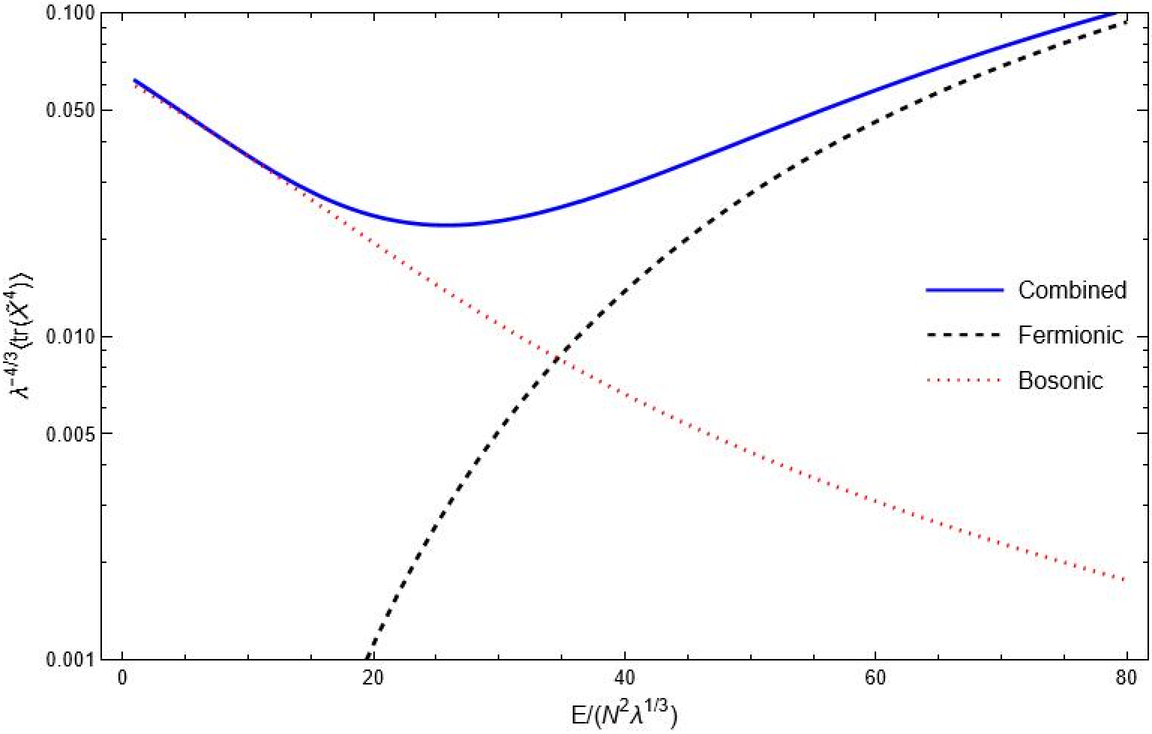

Figure 11: Plot of the lower bounds of $\langle \mathrm{tr}(\tilde{X}^4)\rangle$ from the bosonic components (purple/dotted), fermionic components (orange/dashed), and both (blue/solid). Note that the bosonic and fermionic contributions are higher at low and high energies respectively.

	O	X	P
O	$\frac{1}{9}\langle \mathrm{Tr}(O^I O_I)\rangle$	$\frac{2}{9}\left(\frac{1}{3}E - \langle \mathcal{B}\rangle\right)$	0
X	$\frac{2}{9}\left(\frac{1}{3}E - \langle \mathcal{B}\rangle\right)$	$\langle \mathrm{Tr}(X^2)\rangle$	$-i\frac{N^2}{2}$
P	0	$i\frac{N^2}{2}$	$\frac{2}{9}\left(\frac{1}{3}E + \langle \mathcal{B}\rangle\right)$

Table 6: Bootstrap matrix using an arbitrary position, momentum, and fermionic matrix. Note that the upper-left submatrix corresponds to the fermionic contribution, while the bottom-right submatrix is purely bosonic.

where b is the value of $\langle \mathcal{B}\rangle$ at the boundary itself. We can get rid of the b dependence in this inequality by minimizing its right hand side with respect to b, since we are looking for a lower bound. This purely fermionic constraint for $\langle \mathrm{tr}(\tilde{X}^2)\rangle$ can be found in Figure 12.

To get a bound on $\langle \mathrm{tr}(\tilde{X}^4)\rangle$ instead, like we did with the bosonic matrices, we can invoke the simple identity $\langle \mathrm{tr}(\tilde{X}^4)\rangle \geq \langle \mathrm{tr}(\tilde{X}^2)\rangle^2$. If we use the positivity constraint on solely the 2×2 upper sub matrix of Table 11, we get a purely fermionic lower bound:

$$64\langle \mathrm{tr}(\tilde{X}^2)\rangle \geq \frac{4}{9}\left(\frac{\varepsilon}{9} - \frac{8}{3}\langle \mathrm{tr}(\tilde{X}^2)\rangle^2\right)^2. \tag{88}$$

The lower bound of $\langle \mathrm{tr}(\tilde{X}^4)\rangle$ using the above equation can be found in Figure 11.

We can also incorporate bosonic terms into this constraint to find a stronger bound. From eqn. (84), we see that we can set $b = 72\langle \mathrm{tr}(\tilde{X}^4)\rangle$ at the boundary[14]. Setting the right hand side of eqn. (87), which uses the positivity constraint on the entirety of Table 6, equal to $b/72$

[14] One may use the value for b from minimizing eqn. (87). However, this produces a weaker bound.

yields a combined lower bound:

$$\left(\frac{\varepsilon}{9}+\frac{b}{3}\right)\left[12\sqrt{2}\sqrt{b}-\left(\frac{\varepsilon}{9}-\frac{b}{3}\right)^2\right]=54. \tag{89}$$

This lower bound matches the bosonic and fermionic constraints at low and high energies respectively, as seen in Figure 11. The most noticeable difference is in the middle of these values, where the combined lower bound is higher.

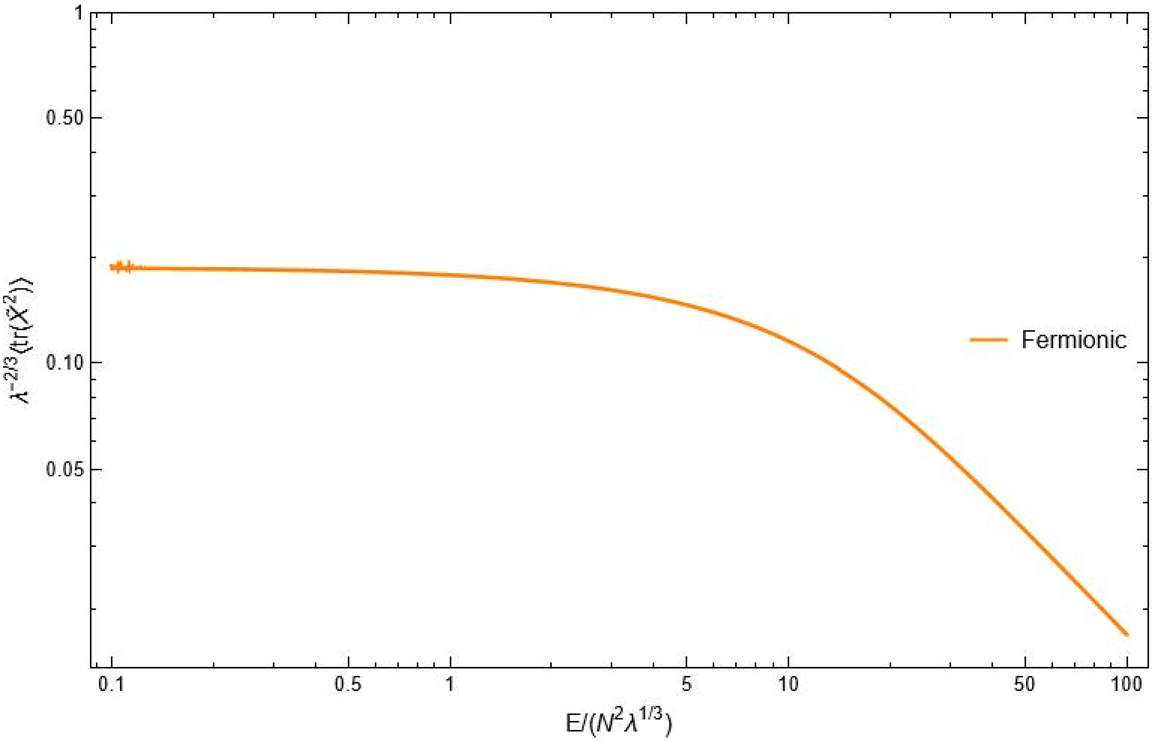

Figure 12: Plot of the lower bound of $\langle \mathrm{tr}(\tilde{X}^2)\rangle$ from the fermionic components. There is no trivial bound from the bosonic terms.

The simple bootstrap matrices used thus far have produced bounds on these observables that were found through much more complex Monte Carlo methods [34, 35, 36, 37]. Using larger matrices, like in Section 4.1, will yield better bounds. In addition, a myriad of properties have yet to be used, such as supersymmetry, the large N approximation, and SU(N) gauge symmetry. A more depth discussion of the above method - both strengths and weaknesses - can be found in [11].

5. Summary and Conclusion

The above work showcases our work from the summer. As stated previously, a considerable amount of time and effort went into understanding the method of bootstrap as a whole. This included studying various single particle systems, such as the harmonic oscillator, Pöschl-Teller potential, and $\mathcal{PT}$ symmetric systems. Our graphs matched those from existing literature, which suggests that we have utilized the bootstrap method in the correct way.

Since this research is concerned with holography, the connection between a gravitational and non-gravitational theory, we turned our attention towards studying quasinormal modes of various black hole metrics. We found analytical forms of these modes for 2+1 dimensional settings, such as the AdS_3 spacetime and BTZ black hole, while we used a semi-analytical approach for the 3+1 Schwarzschild black hole, which does not have an analytical solution for its wave function.

We then turned our attention to matrix models, since our end-goal is to understand the D0-Brane Matrix Model. We started with the Anharmonic Oscillator Matrix Model, which we were able to compare with the exact energy levels to gauge the accuracy of the bootstrap method. Finally, we turned to the D0-Brane Matrix Model. Here, we used the bosonic and fermionic components to derive constraints on the energy levels with respect to observables such as $\langle \mathrm{tr}(\tilde{X}^l) \rangle$.

Our next steps is to resolve issues encountered in the above examples. More specifically, we would like to use the new metric from eqn. (69) to determine if a normalizable wave function can be found. In addition, we would like to derive bootstrap constraints using strings of length ≤ 3 for the Anharmonic Oscillator Matrix Model.

After finishing up with the examples, we would like to study two main facets of the D0-Brane Matrix Model. It has been found that for $N = 2$, there are zero bound energy states. However, an analytical proof for $N \geq 3$ has not been found due to the complexity of the problem. Thus, we hope that bootstrapping the system will provide information about the bound states. Furthermore, we would like to study quasinormal modes of the 10 dimensional black hole that the D0-Brane Matrix Model relates to in the 't Hooft limit, which has already been done in the super-gravity side but not the matrix side. Finding these would correspond to studying correlator functions $\langle X^l(t) X^l(t') \rangle$ in the matrix setting.

Acknowledgments

The author would like to thank Professor Mukund Rangamani for his guidance throughout this project. The author also appreciates Dr. Christian Ferko for his helpful discussions. The author further acknowledges support from the National Science Foundation from its REU Site in Physics and Astronomy (NSF Grant No. PHY-2150515) at University of California Davis.

References

[1] Elias Kiritsis. *String theory in a nutshell*, volume 21. Princeton University Press, 2019.

[2] Juan Maldacena. The large-n limit of superconformal field theories and supergravity. *International journal of theoretical physics*, 38(4):1113–1133, 1999.

[3] Veronika E Hubeny. The ads/cft correspondence. *Classical and Quantum Gravity*, 32(12): 124010, 2015.

[4] Gary T Horowitz. Comments on black holes in string theory. *Classical and Quantum Gravity*, 17(5):1107, 2000.

[5] Sebastian de Haro. Quantum gravity and the holographic principle. *arXiv preprint hep-th/0107032*, 2001.

[6] Tom Banks, Willy Fischler, Steven H Shenker, and Leonard Susskind. M theory as a matrix model: A conjecture. In *The World in Eleven Dimensions*, pages 435–451. CRC Press, 1999.

[7] Anna Biggs and Juan Maldacena. Scaling similarities and quasinormal modes of d0 black hole solutions. *Journal of High Energy Physics*, 2023(11):1–30, 2023.

[8] Jan Dereziński and Michał Wrochna. Exactly solvable schrödinger operators. In *Annales Henri Poincaré*, volume 12, pages 397–418. Springer, 2011.

[9] Martin Kruczenski, Joao Penedones, and Balt C van Rees. Snowmass white paper: S-matrix bootstrap. *arXiv preprint arXiv:2203.02421*, 2022.

[10] Miguel F Paulos, Joao Penedones, Jonathan Toledo, Balt C Van Rees, and Pedro Vieira. The s-matrix bootstrap. part i: Qft in ads. *Journal of High Energy Physics*, 2017(11): 1–45, 2017.

[11] Henry W Lin. Bootstrap bounds on d0-brane quantum mechanics. *Journal of High Energy Physics*, 2023(6):1–19, 2023.

[12] David Berenstein and George Hulsey. Bootstrapping simple qm systems. *arXiv preprint arXiv:2108.08757*, 2021.

[13] Carl M Bender and Stefan Boettcher. Real spectra in non-hermitian hamiltonians having p t symmetry. *Physical review letters*, 80(24):5243, 1998.

[14] Carl M Bender. Introduction to $\mathcal{PT}$-symmetric quantum theory. *Contemporary physics*, 46(4):277–292, 2005.

[15] Carl M Bender, Dorje C Brody, and Hugh F Jones. Extension of pt-symmetric quantum mechanics to quantum field theory with cubic interaction. *Physical Review D*, 70(2):025001, 2004.

[16] Carl M Bender and Hugh F Jones. Semiclassical calculation of the c operator in pt-symmetric quantum mechanics. *Physics Letters A*, 328(2-3):102–109, 2004.

[17] Philip D Mannheim. Appropriate inner product for pt-symmetric hamiltonians. *Physical Review D*, 97(4):045001, 2018.

[18] Carl M Bender and Hugh F Jones. Interactions of hermitian and non-hermitian hamiltonians. *Journal of Physics A: Mathematical and Theoretical*, 41(24):244006, 2008.

[19] Sakil Khan, Yuv Agarwal, Devjyoti Tripathy, and Sachin Jain. Bootstrapping pt symmetric hamiltonians. *arXiv preprint arXiv:2202.05351*, 2022.

[20] Hugh F Jones and J Mateo. Equivalent hermitian hamiltonian for the non-hermitian $-x^4$ potential. *Physical Review D—Particles, Fields, Gravitation, and Cosmology*, 73(8): 085002, 2006.

[21] Grigoris Panotopoulos. Quasinormal modes of the btz black hole under scalar perturbations with a non-minimal coupling: exact spectrum. *General Relativity and Gravitation*, 50(6): 59, 2018.

[22] Vitor Cardoso and Jose PS Lemos. Scalar, electromagnetic, and weyl perturbations of btz black holes: Quasinormal modes. *Physical Review D*, 63(12):124015, 2001.

[23] Yasuyuki Hatsuda and Masashi Kimura. Spectral problems for quasinormal modes of black holes. *Universe*, 7(12):476, 2021.

[24] Masashi Kimura. Note on the parametrized black hole quasinormal ringdown formalism. *Physical Review D*, 101(6):064031, 2020.

[25] Yasuyuki Hatsuda and Masashi Kimura. Semi-analytic expressions for quasinormal modes of slowly rotating kerr black holes. *Physical Review D*, 102(4):044032, 2020.

[26] GA Baker Jr and PR Graves-Morris. Padé approximants. encycl. math. vol. 59, 1996.

[27] Tin Sulejmanpasic and Mithat Ünsal. Aspects of perturbation theory in quantum mechanics: The benderwu mathematica® package. *Computer Physics Communications*, 228:273–289, 2018.

[28] Carl M Bender and Tai Tsun Wu. Anharmonic oscillator. *Physical Review*, 184(5):1231, 1969.

[29] Xizhi Han, Sean A Hartnoll, and Jorrit Kruthoff. Bootstrapping matrix quantum mechanics. *Physical Review Letters*, 125(4):041601, 2020.

[30] Edouard Brézin, Claude Itzykson, Giorgio Parisi, and Jean-Bernard Zuber. Planar diagrams. *Communications in Mathematical Physics*, 59:35–51, 1978.

[31] Juan Maldacena and Alexey Milekhin. To gauge or not to gauge? *Journal of High Energy Physics*, 2018(4):1–36, 2018.

[32] Juan Maldacena. A simple quantum system that describes a black hole. *arXiv preprint arXiv:2303.11534*, 2023.

[33] Joseph Polchinski. M-theory and the light cone. *Progress of Theoretical Physics Supplement*, 134:158–170, 1999.

[34] Daniel Kabat, Gilad Lifschytz, and David Lowe. Black hole thermodynamics from calculations in strongly coupled gauge theory. *International Journal of Modern Physics A*, 16 (05):856–865, 2001.

[35] Konstantinos N Anagnostopoulos, Masanori Hanada, Jun Nishimura, and Shingo Takeuchi. Monte carlo studies of supersymmetric matrix quantum mechanics with sixteen supercharges at finite temperature. *Physical review letters*, 100(2):021601, 2008.

[36] Masanori Hanada, Yoshifumi Hyakutake, Jun Nishimura, and Shingo Takeuchi. Higher derivative corrections to black hole thermodynamics<? format?> from supersymmetric matrix quantum mechanics. *Physical review letters*, 102(19):191602, 2009.

[37] Denjoe O'Connor. The bfss model on the lattice. *Journal of High Energy Physics*, 2016 (05):167, 2016.

A. Bootstrap Constraints for the Anharmonic Oscillator

The table with all strings with length $L \leq 2$ is:

	I	X^2	P^2	XP	PX	X	P
I	N	$\langle \mathrm{Tr}(X^2)\rangle$	$\langle \mathrm{Tr}(P^2)\rangle$	$\langle \mathrm{Tr}(XP)\rangle$	$\langle \mathrm{Tr}(PX)\rangle$		
X^2	$\langle \mathrm{Tr}(X^2)\rangle$	$\langle \mathrm{Tr}(X^4)\rangle$	$\langle \mathrm{Tr}(P^2X^2)\rangle$	$\langle \mathrm{Tr}(XPX^2)\rangle$	$\langle \mathrm{Tr}(PX^3)\rangle$		
P^2	$\langle \mathrm{Tr}(P^2)\rangle$	$\langle \mathrm{Tr}(X^2P^2)\rangle$	$\langle \mathrm{Tr}(P^4)\rangle$	$\langle \mathrm{Tr}(XP^3)\rangle$	$\langle \mathrm{Tr}(PXP^2)\rangle$		
PX	$\langle \mathrm{Tr}(PX)\rangle$	$\langle \mathrm{Tr}(X^2PX)\rangle$	$\langle \mathrm{Tr}(P^3X)\rangle$	$\langle \mathrm{Tr}(XP^2X)\rangle$	$\langle \mathrm{Tr}(PXPX)\rangle$		
XP	$\langle \mathrm{Tr}(XP)\rangle$	$\langle \mathrm{Tr}(X^3P)\rangle$	$\langle \mathrm{Tr}(P^2XP)\rangle$	$\langle \mathrm{Tr}(XPXP)\rangle$	$\langle \mathrm{Tr}(PX^2P)\rangle$		
X						$\langle \mathrm{Tr}(X^2)\rangle$	$\langle \mathrm{Tr}(PX)\rangle$
P						$\langle \mathrm{Tr}(XP)\rangle$	$\langle \mathrm{Tr}(P^2)\rangle$

The empty elements indicates 0. To simplify this matrix and reduce the degrees of freedom, we use the four constraints outlined in Section 4:

1. $\langle [H, \mathcal{O}]\rangle = 0$, $\mathcal{O} \in \mathcal{S}_{2L}$
2. $\langle \mathrm{Tr}(G\mathcal{O})\rangle = 0$, $\mathcal{O} \in \mathcal{S}_{2L-2}$
3. $\langle \mathcal{O}^\dagger \rangle = \langle \mathcal{O}\rangle^*$, $\mathcal{O} \in \mathcal{S}_{2L}$
4. Cyclicity of the Trace,

where $H = \mathrm{Tr}(P^2) + \mathrm{Tr}(X^2) + \frac{g}{N}\,\mathrm{Tr}(X^4)$ and $G = i[X,P] + NI$ for the Anharmonic Oscillator with $N \times N$ position/momentum matrices. In addition, let us define $\mathcal{S}_k$ as the set of all strings with length $\leq k$. From previous work, we know that $\langle \mathrm{Tr}(XP)\rangle = -\langle \mathrm{Tr}(PX)\rangle = \frac{iN^2}{2}$. We also know that $\langle \mathrm{Tr}(P^2)\rangle = \langle \mathrm{Tr}(X^2)\rangle + \frac{2g}{N}\,\langle \mathrm{Tr}(X^4)\rangle$. Our objective is to write everything else in terms of the traces of X^2, X^4, and other unattainable quantities.

First, let us work with $XPXP, PXPX, XP^2X$, and PX^2P. Using the second and third identities, we see that

$$\begin{aligned}\langle \mathrm{Tr}(XPXP)\rangle &= \langle \mathrm{Tr}(PX^2P)\rangle - \frac{N^3}{2},\\ \langle \mathrm{Tr}(PXPX)\rangle &= \langle \mathrm{Tr}(XP^2X)\rangle - \frac{N^3}{2}.\end{aligned} \tag{90}$$

We know that $(PX^2P)^\dagger = PX^2P$, so $\langle \mathrm{Tr}(PX^2P)\rangle \in \mathbb{R}$. The same thing applies for $\langle \mathrm{Tr}(XP^2X)\rangle$. Thus, both $\langle \mathrm{Tr}(XPXP)\rangle = \langle \mathrm{Tr}(PXPX)\rangle \in \mathbb{R}$, since $\langle \mathrm{Tr}((XPXP)^\dagger)\rangle = \langle \mathrm{Tr}(PXPX)\rangle$. Furthermore, using cyclicity of trace with $\langle \mathrm{Tr}(PX^2P)\rangle$ and $\langle \mathrm{Tr}(XP^2X)\rangle$, we find

$$\begin{aligned}\langle \mathrm{Tr}(XP^2X)\rangle &= \langle \mathrm{Tr}(P^2X^2)\rangle + \frac{N^3}{2},\\ \langle \mathrm{Tr}(PX^2P)\rangle &= \langle \mathrm{Tr}(X^2P^2)\rangle + \frac{N^3}{2}.\end{aligned} \tag{91}$$

This of course means that $\langle \mathrm{Tr}(P^2X^2)\rangle = \langle \mathrm{Tr}(PXPX)\rangle = \langle \mathrm{Tr}(X^2P^2)\rangle$.

Constraint	Operators
$\langle [H, \mathcal{O}]\rangle$	XP, PX, X^4
$\langle \mathrm{Tr}(G\mathcal{O})\rangle$	$\mathcal{S}_2$
$\langle \mathrm{Tr}(\mathcal{O}^\dagger)\rangle = \langle \mathrm{Tr}(\mathcal{O})\rangle^*$	$\mathcal{S}_4$
Cyclicity of Trace	$\mathcal{S}_4 - \mathcal{S}_2$

Table 7: Table of all operators that were used for each constraint. Operators that produced a string with length $L \geq 6$ were not considered.

Next, we focus on $\langle \mathrm{Tr}(PX^3)\rangle$ and its adjacent terms. From the cyclicity of trace, the Hamiltonian (with $\mathcal{O} = X^4$), and generator constraints, we see that

$$\begin{aligned}\langle \mathrm{Tr}(PX^3)\rangle &= \langle \mathrm{Tr}(X^3P)\rangle - 2iN\langle \mathrm{Tr}(X^2)\rangle,\\ \langle \mathrm{Tr}(PX^3)\rangle &= -\langle \mathrm{Tr}(X^3P)\rangle,\\ \langle \mathrm{Tr}(PX^3)\rangle &= \langle \mathrm{Tr}(XPX^2)\rangle - iN\langle \mathrm{Tr}(X^2)\rangle.\end{aligned} \tag{92}$$

These imply that $\langle \mathrm{Tr}(PX^3)\rangle = -iN\langle \mathrm{Tr}(X^2)\rangle$ and $\langle \mathrm{Tr}(XPX^2)\rangle = 0$. Then, $\langle \mathrm{Tr}(X^2PX)\rangle = 0$ as well.

The only terms we have not considered are $\langle \mathrm{Tr}(XP^3)\rangle$ and its corresponding terms. From the cyclicity of trace and generator constraints, we find

$$\begin{aligned}\langle \mathrm{Tr}(XP^3)\rangle &= \langle \mathrm{Tr}(P^3X)\rangle + 2iN\langle \mathrm{Tr}(P^2)\rangle,\\ \langle \mathrm{Tr}(XP^3)\rangle &= \langle \mathrm{Tr}(PXP^2)\rangle + iN\langle \mathrm{Tr}(P^2)\rangle.\end{aligned} \tag{93}$$

Let $e = x + iy = \langle \mathrm{Tr}(XP^3)\rangle$. Then, if we take the conjugate of both sides of the second equation above, then we see that

$$(x+iy)^* = \langle \mathrm{Tr}(P^3X)\rangle = \langle \mathrm{Tr}(P^2XP)\rangle - iN\langle \mathrm{Tr}(P^2)\rangle. \tag{94}$$

meaning $\langle \mathrm{Tr}(P^2XP)\rangle = x + iy - iN\langle \mathrm{Tr}(P^2)\rangle = \langle \mathrm{Tr}(PXP^2)\rangle$, making both of these terms real. This means $y = iN\langle \mathrm{Tr}(P^2)\rangle$.

The updated table can be found in Table 3. Table 7 outlines which operators were used for each constraint. Operators with a total odd power are not considered since the Hamiltonian is even. In addition, note that we cannot find $\langle \mathrm{Tr}(X^2)\rangle$,$\langle \mathrm{Tr}(X^4)\rangle$, $\langle \mathrm{Tr}(P^4)\rangle$, and $\langle \mathrm{Tr}(XPXP)\rangle$ without involving strings of length $L = 6$.